ACS NANO

www.acsnano.org

ARTICLE

Nanoparticle-Driven Tendon Repair: Role of Vasoactive Intestinal Peptide in Immune Modulation and Stem Cell Enhancement

Hao Wang,‡ Yucheng Gao,‡ Jinyu Wang,‡ Mumin Cao, Guangchun Dai, Panpan Lu, Renwang Sheng, Cheng Zhang, Qianqian Wang, Gang Li, Qi Yong H. Ai, Yunfeng Rui,* and Liu Shi*

Cite This: *ACS Nano* 2025, 19, 13871−13888

Read Online

ACCESS | Metrics & More | Article Recommendations | Supporting Information

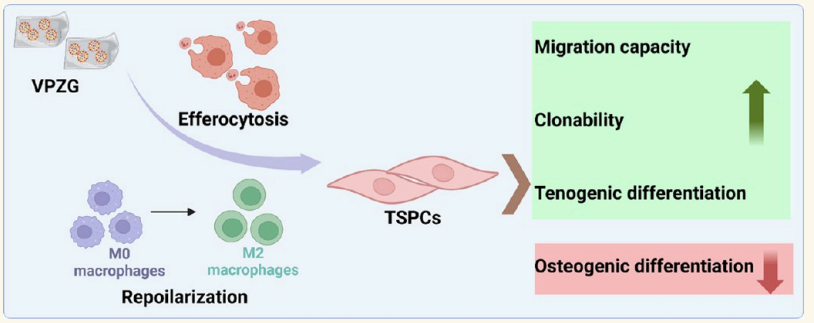

ABSTRACT: **Tendon repair remains challenging owing to the limited capacity for endogenous repair. Vasoactive intestinal peptide (VIP) promotes bone tissue regeneration; however, its role in tendon repair remains unclear. In the present study, we demonstrated that VIP stimulated M2 polarization of macrophages and facilitated tendon regeneration by regulating immune homeostasis and maintaining the function of tendon stem/progenitor cells (TSPCs). Additionally, we established GelMa-loaded VIP@PLGA@ZIF-8 (VPZ) nanoparticles (VPZG) to enable the sustained and localized release of VIP at the site of patellar tendon injury in SD rats. The results of the *in vitro* experiments demonstrated that VPZG regulated the homeostasis of macrophage polarization by downregulating the NF-κB axis. VPZG also promoted efferocytosis and suppressed the release of proinflammatory factors. Additionally, VPZG enhanced the tenogenic differentiation of TSPCs when cocultured with macrophages. *In vivo*, we implanted VPZG at the site of patellar tendon injury, where it released VIP sustainably and slowly to promote tendon regeneration. This effect was achieved through the downregulation of the expression levels of various inflammatory factors, as well as the regulation of local immune homeostasis. In conclusion, our results demonstrated that VPZG facilitated tendon injury repair by regulating immune homeostasis and enhancing TSPC function. These findings suggest that VPZG is a promising avenue for the clinical improvement of tendon injury treatment.**

KEYWORDS: *vasoactive intestinal peptide, tendon regeneration, polarization, tendon stem/progenitor cells, inflammatory microenvironment*

Downloaded via KOREA UNIV on October 31, 2025 at 02:58:27 (UTC).
See https://pubs.acs.org/sharingguidelines for options on how to legitimately share published articles.

INTRODUCTION

Tendons are important tissues that connect muscles to bones, transmitting force and enabling body movements. Tendon injuries are common in both athletic and nonathletic individuals and affect the quality of life of the patients. These injuries are particularly common during high-intensity exercises and repetitive loading.[1] Trauma, aging,[2,3] diabetes,[4] and overuse are potential risk factors for tendon injuries. These injuries not only cause great inconvenience to individuals and families but also impose economic burdens on society.[5] Unfortunately, tendons exhibit a limited capacity for self-repair. Moreover, current conservative treatments, such as corticosteroid injections and shockwave therapy, and surgical treatments demonstrate limited effectiveness.[6,7] Conservative treatments typically involve a prolonged recovery period and

Received: November 25, 2024
Revised: March 27, 2025
Accepted: March 28, 2025
Published: April 4, 2025

ACS Publications © 2025 American Chemical Society

Scheme 1. Regulation of Immune and Stem Cell Homeostasis to Promote Healing of Patellar Tendon Injuries by VPZG[a]

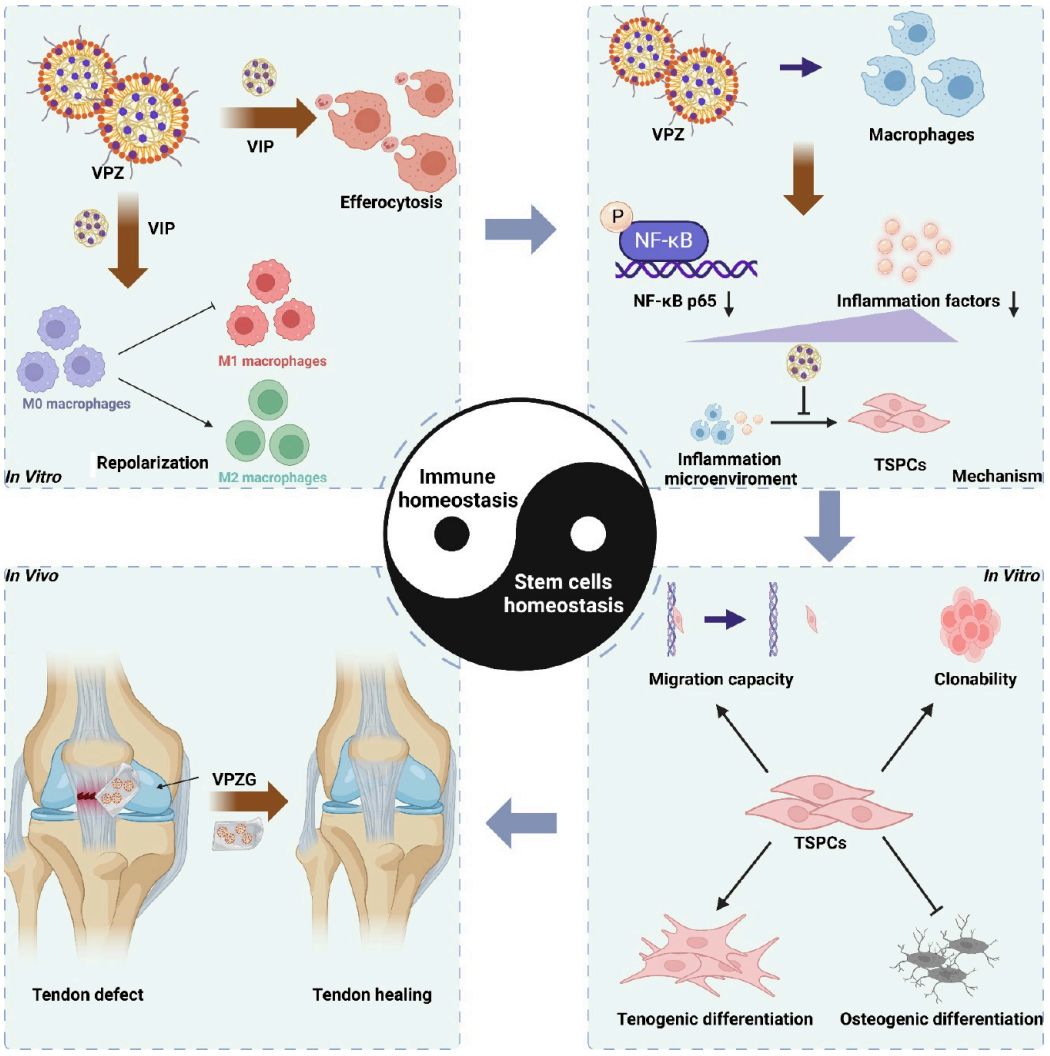

[a]VPZ, VIP@PLGA@ZIF-8@GelMa; GelMa-loaded VIP@PLGA@ZIF-8; VPZG, VPZ nanoparticle; VIP, vasoactive intestinal peptide; TSPCs, tendon stem/progenitor cells.

cannot fully restore tendon structure and function. Although surgical repair can reconstruct the tendon structure, it is associated with complications such as infection, tendon adhesions, and rerupture. Therefore, treatments that can effectively promote tendon regeneration and repair are urgently required.

Macrophage polarization-mediated immune homeostasis plays a crucial role in tissue repair and regenerative medicine.[8] This process is characterized by the balance between M1 and M2 polarizations. M1 macrophages are proinflammatory, initiating inflammatory infiltration and recruitment, whereas M2 macrophages promote tissue repair. Disruption of macrophage polarization homeostasis and impaired macrophage function may contribute to the limited regenerative capacity of tendons. Macrophage M2 polarization promotes tissue repair by regulating the levels of inflammatory factors in the injured region and modulating stem cell behavior.[9,10] Notably, the functional maintenance of tendon stem/progenitor cells (TSPCs) depends on the regulation of the immune microenvironment,[11] particularly macrophage polarization.[12] Promoting M2 macrophage polarization enhances TSPC proliferation, migration, and tenogenic differentiation, thereby accelerating tendon injury repair.[13] Furthermore, preserving immune homeostasis is crucial for preventing TSPC senescence and functional decline. This contributes to improved repair and long-term stability of tendon tissue. Therefore, modulating immune homeostasis and stem cell fate could be a key therapeutic strategy for tendon regeneration.

The nervous system plays an active role in pain regulation, inflammation, and tissue repair via efferent pathways. Vasoactive intestinal peptide (VIP) is a neuropeptide derived from the sympathetic nervous system. It has gained attention for its potential role in tissue regeneration, particularly in modulating inflammation and immune responses. VIP exhibits strong anti-inflammatory effects, modulating both proinflammatory and anti-inflammatory cytokine profiles.[14] VIP can prevent rheumatoid arthritis by downregulating the inflammatory response.[15] Moreover, recent studies have highlighted the role of VIP in various tissue regeneration processes, including bone and nerve. For example, VIP promotes osteogenesis and bone regeneration by reducing the secretion of inflammatory cytokines and promoting the recruitment of progenitor cells in bone tissues.[16] Similarly, in nerve repair, VIP demonstrates neuroprotective effects by enhancing nerve regeneration and

https://doi.org/10.1021/acsnano.4c16917
ACS Nano 2025, 19, 13871−13888

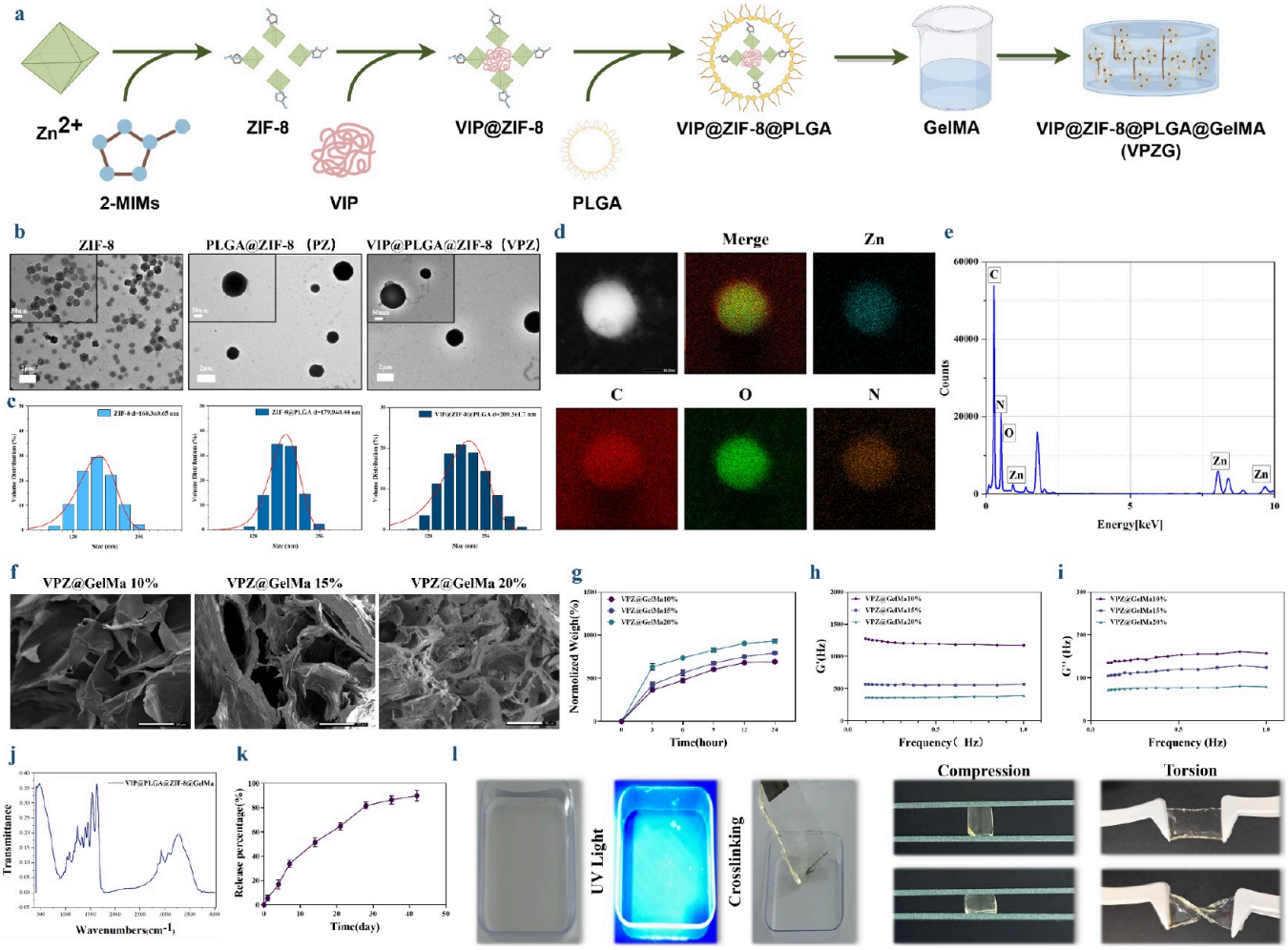

Figure 1. Characterization of VPZ and VPZG. (a) Schematic of VPZG synthesis process. (b) Transmission electron microscopy images and (c) particle size of ZIF-8, PZ, and VPZ. Scale bar, 2 μm. (d) Transmission electron microscope images and (e) energy spectra of VPZ. Scale bar, 50 nm. (f) Scanning electron microscopy images of VPZ added at different concentrations (10, 15, and 20%) of GelMa. Scale bar, 10 μm. (g) Swelling test at 10, 15, 20% VPZ@GelMa. Rotational rheometer measurements of the (h) storage modulus and (i) loss modulus of hydrogels. (j) Fourier-transform infrared spectra of VPZG. (k) Drug release of VPZG. (h) Cross-linking, compressing, and torsion processes of 20% VPZ@GelMa. VPZ, VIP@PLGA@ZIF-8@GelMa; GelMa-loaded VIP@PLGA@ZIF-8; VPZG, VPZ nanoparticles.

reducing inflammation.[17,18] Our previous studies have confirmed the potential of VIP application in bone tissue regeneration. VIPs play an important role in innervation during early bone development and bone repair.[19−21] However, its application in tendon repair, particularly its effects on TSPCs and macrophage polarization, remains an area of ongoing research, with few studies directly addressing its impact on tendon regeneration.

We hypothesized that VIP could contribute to tendon repair by modulating the inflammatory response at the site of injury. The inflammatory microenvironment forms and develops at the site of tendon injury and occurs throughout the repair process. Therefore, establishing an effective slow-release drug system that continuously regulates this inflammatory microenvironment presents another challenge in tendon regeneration engineering. Nanomaterials were widely used as important biomaterials in the regenerative field owing to their efficient drug-loading and slow-release properties.[22] Therefore, in the present study, we prepared PLGA@ZIF-8 nanoparticles using an emulsification method to improve the drug-loading rate and slow-release ability. Specifically, we established a VIP@PLGA@ZIF-8@GelMa (VPZG) hydrogel system and implanted it at the tendon injury site in a rat patellar tendon injury model.[23] Our results demonstrated that VPZG sustains macrophage M2 polarization and ultimately modulates the inflammatory microenvironment by slowly releasing VIP at the injury site. Mechanistically, VPZG promotes M2 polarization by downregulating the NF-κB signaling pathway to reduce the expression of proinflammatory factors in macrophages, as well as by enhancing efferocytosis. Additionally, we cocultured macrophages with tendon stem cells *in vitro* and demonstrated that VIP promotes the migration, proliferation, and tenogenic differentiation of TSPCs by modulating the inflammatory microenvironment. Overall, our study demonstrates the role of VIP in promoting tendon injury repair and the potential application of the VPZG system in tendon regeneration (Schematic 1).

RESULTS

Characterization of VPZ and VPZG. The synthetic schemes for VPZ and VPZG are depicted in Figure 1a. We examined the morphologies of ZIF-8, PLGA@ZIF-8 (PZ), and VPZ using transmission electron microscopy (TEM) (Figure 1b). PZ and VPZ exhibited regular circular shapes with particle

https://doi.org/10.1021/acsnano.4c16917
ACS Nano 2025, 19, 13871−13888

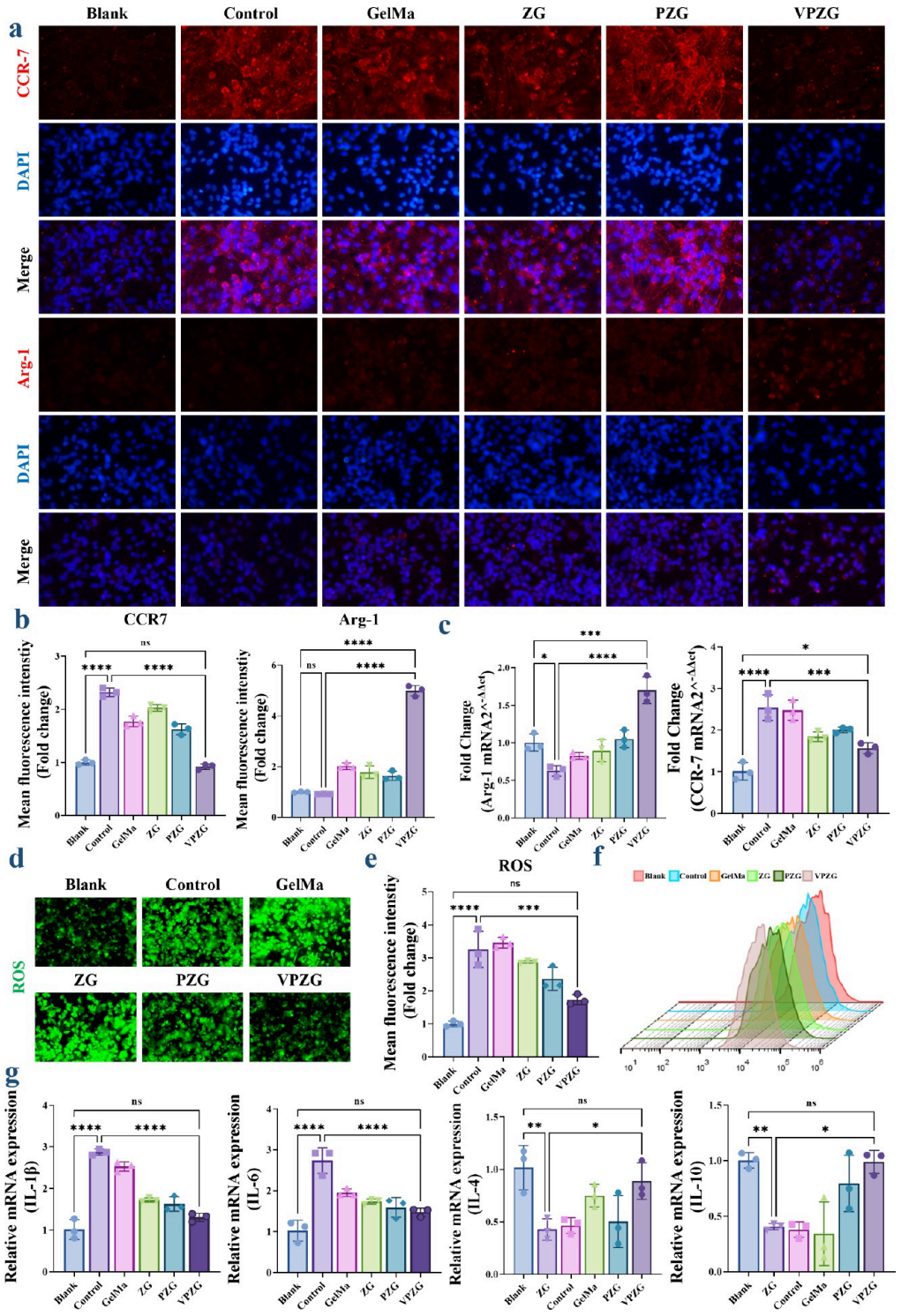

Figure 2. VPZG Promotes M2Macrophage Polarization*in vitro*. (a) Immunofluorescence and (b) semiquantitative analysis of the M1 marker CCR7 and the M2 marker Arg-1 after treatment of THP-1 with VPZG. (c) qPCR analysis of the relative mRNA expression levels of *CCR-7* and *ARG-1* in THP-1 treat with VPZG. (d) Fluorescence imaging and (e) semiquantitative analysis of intracellular ROS levels in macrophages. (f) Flow cytometry analysis of intracellular ROS after coincubation of different groups of macrophages. (g) qPCR analysis of the relative mRNA expression levels of cellular proinflammatory factors (*IL-1B* and *IL-6*) and anti-inflammatory factors (*IL-4* and *IL-10*) after VPZG treatment of THP-1 cells. *$p < 0.05$, **$p < 0.01$, ***$p < 0.001$, ****$p < 0.0001$, ns: no significance. Expressed as mean ± SEM or SD. VPZ, VIP@PLGA@ZIF-8@GelMa; GelMa-loaded VIP@PLGA@ZIF-8; VPZG, VPZ nanoparticle; ROS, reactive oxygen species; GelMa, LPS + GelMa added; ZG, with LPS+ZIF-8@GelMa added; PZG, with LPS+PLGA@ZIF-8@GelMa; and VPZG, with LPS+VIP@PLGA@ZIF-8@GelMa added.

sizes of 179.9 and 209.3 nm, respectively, and were uniformly dispersed (Figure 1c). The particle size increased to a certain extent after PLGA coating and VIP loading. Energy dispersive X-ray spectroscopy mapping revealed the distribution of Zn, C,

https://doi.org/10.1021/acsnano.4c16917
ACS Nano 2025, 19, 13871−13888

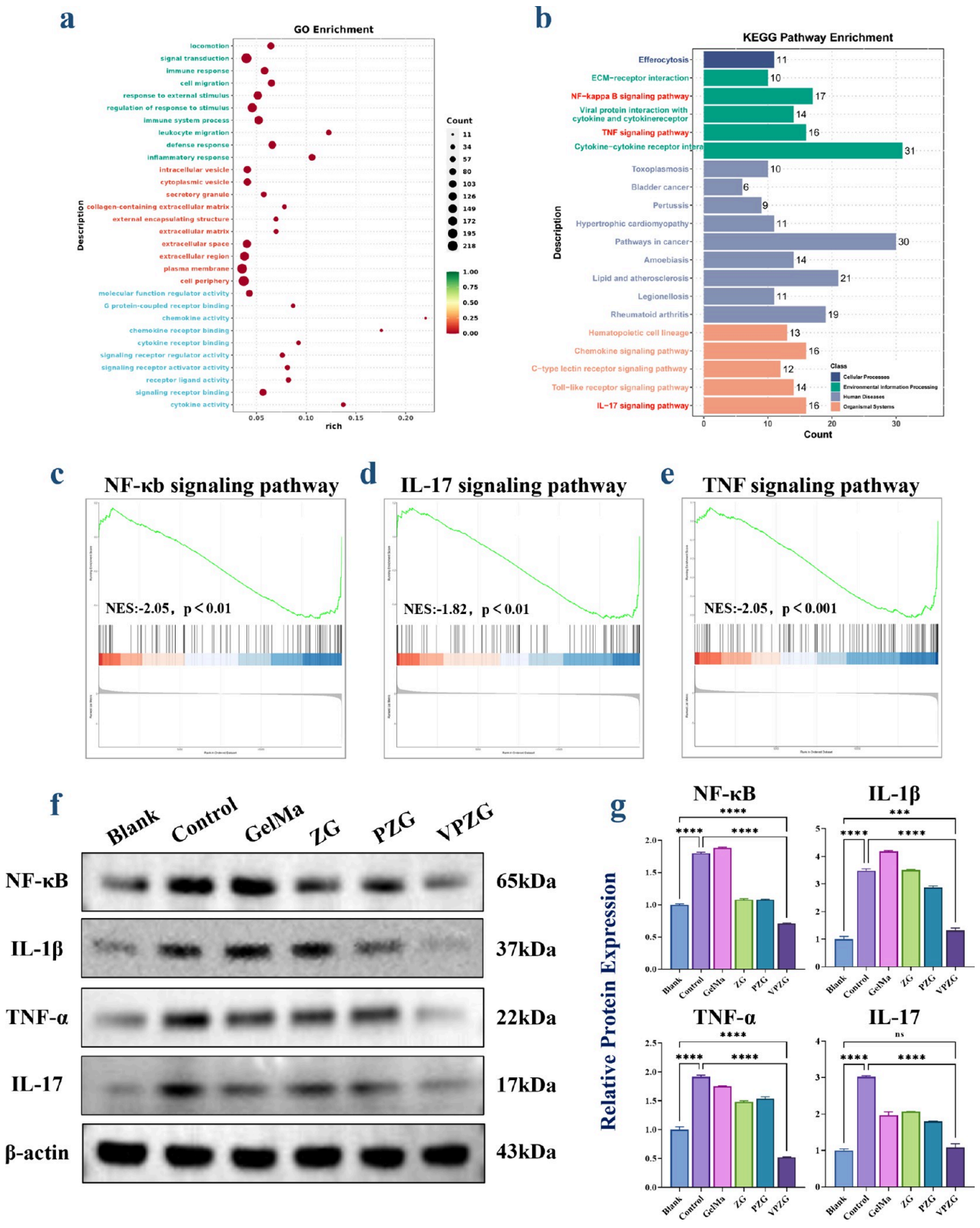

Figure 3. VPZG Regulates Macrophage Repolarization via the NF-κB Signaling Pathway. (a) Top 30 differential Gene Ontology enrichment pathways after treatment with VPZG compared to control and (b) top 20 Kyoto Encyclopedia of Genes and Genome enrichment pathway. Gene set enrichment analysis of the (c) NF-KB signaling pathway, (d) IL-17 signaling pathway, and (e) TNF-α signaling pathway in the VPZG group compared to the control group. (f) Western blotting of the changes in the expression levels of macrophage NF-κB, IL-1β, IL-17, and TNF-α proteins. (g) Semiquantitative analysis of protein expression. ***$p < 0.001$, ****$p < 0.0001$, ns: no significance. Expressed as mean ± SEM. IL, interleukin; TTNF-α, tumor necrosis factor-alpha; VPZ, VIP@PLGA@ZIF-8@GelMa; GelMa-loaded VIP@PLGA@ZIF-8; VPZG, VPZ nanoparticle; GelMa, LPS + GelMa added; ZG, with LPS+ZIF-8@GelMa added; PZG, with LPS+PLGA@ZIF-8@GelMa; and VPZG, with LPS+VIP@PLGA@ZIF-8@GelMa added.

https://doi.org/10.1021/acsnano.4c16917
ACS Nano 2025, 19, 13871−13888

O, and N, confirming that PLGA was coated onto the surface of ZIF-8 (Figures 1d-e). The average potential of ZIF-8, PLGA@ZIF-8, and protein-loaded PLGA@ZIF-8 was recorded at 3.76 mV, − 4.6 mV, and − 14.2 mV, respectively (Figure S1). The significant decrease in the potential after the PLGA coating was attributed to the negative charge of PLGA, further confirming the successful synthesis of the material.

To select a tendon repair scaffold with optimal performance, we used different concentrations (10, 15, and 20%) of GelMA, resulting in the formation of VPZG. Scanning electron microscopy (SEM) results indicated that the pore size of the hydrogel increased with increasing GelMA concentrations (Figure 1f). Furthermore, the hydrogel reached its maximum swelling ratio after 24 h, which was positively correlated with its concentration. The swelling ratios ranged from 500% to 1000%, with 20% GelMA reaching a swelling ratio of 960%. In contrast, the swelling ratios of the 10% and 15% GelMa samples were approximately 710% and 820%, respectively (Figure 1g). We also performed dynamic rate-scanning rheology tests to assess the viscoelasticity and stability of the hydrogels. The storage modulus (G') was greater than the loss modulus (G'), indicating successful hydrogel formation. As the GelMa concentration increased, the G' value peaked, indicating an enhanced modulus of elasticity (Figure 1h-i). Fourier-transform infrared (FTIR) spectroscopy further confirmed the successful synthesis of VPZG (Figure 1j). The primary absorption peaks were observed at 1078 cm^{-1} (alcohols or ethers), 1236 cm^{-1} (esters or amino compounds), 1333 cm^{-1} (CH2 or CH3 group), 1397 cm^{-1} (hydroxyl group), 1447 cm^{-1} (hydrocarbon class), 1535 cm^{-1} (amines or anilines), 1627 cm^{-1} (unsaturated carbon chain), 2924 cm^{-1} (saturated hydrocarbons), and 3274 cm^{-1} (hydroxyl or amino groups). These peaks indicated the presence of alcohols, esters, amino compounds, and hydrocarbons in the material.

We assessed the release of VPZG into VIP using enzyme-linked immunosorbent assay (ELISA), as illustrated in Figure 1k. The release of VPZG persisted for up to 30 days, with approximately 50% of the drug being released within the first 14 days. Figures 1l and S2 depict the synthesis process and the cross-linking, compression, and torsion properties of VPZG. Overall, these experimental results further confirm the successful synthesis of VPZG.

VPZG Promotes M2 Polarization of Macrophages *In Vitro* While Reducing M1 Polarization. We performed a biosafety test before VPZG bioapplication. The results of the CCK-8 and live/dead assays revealed live (green fluorescence) and dead (red fluorescence) cells in each group (Figure S3). The groups exhibited significant proliferation of live cells over time and very weak intensity of red fluorescence, indicating that VPZG has good cytocompatibility.

Macrophage polarization plays an important role in the repair of tendon tissue injury.[9] To verify the effect of VPZG on macrophage polarization, we treated macrophages with lipopolysaccharide (LPS)[24] and simultaneously established a blank group. The groups were as follows: control, with LPS added to simulate the inflammatory environment of tendon injury; GelMa, with LPS + GelMa added; ZG, with LPS+ZIF-8@GelMa added; PZG, with LPS+PLGA@ZIF-8@GelMa; and VPZG, with LPS+VIP@PLGA@ZIF-8@GelMa added. We then investigated the effects of VPZG on macrophage polarization by analyzing the expression of the M1 marker CCR7 and M2 marker Arg-1 via immunofluorescence. Immunofluorescence staining and relative semiquantitative fluorescence analysis indicated that LPS increased CCR7 expression, promoting macrophage M1 polarization, which is involved in the cellular proinflammatory response. However, following treatment with VPZG, Arg-1 expression significantly increased while CCR7 expression significantly decreased compared to those of the control group (Figure 2a-b). We also detected the mRNA levels of *CCR7* and *ARG-1* using quantitative polymerase chain reaction (qPCR) in each group. The results indicated that *ARG-1* mRNA expression increased while *CCR7* mRNA expression decreased after treatment with VPZG in THP-1 cells compared to those of the control group (Figure 2c). These results suggest that VPZG promotes M2 and reduces M1 polarization in macrophages *in vitro*.

Inflammatory factors can increase reactive oxygen species (ROS) expression in macrophages. This increase in ROS can trigger the secretion of inflammatory mediators, disrupting the functional homeostasis of TSPCs in tendon tissue. Therefore, we analyzed ROS expression levels in each group via immunofluorescence using a 2′, 7′-dichlorofluorescein diacetate (DCFH-DA) fluorescent probe. LPS impeded the accumulation of intracellular ROS in macrophages compared to the blank group. However, in the GelMa, ZG, and PZG groups, we observed no reduction in the ROS content in the macrophages. In contrast, the VPZG treatment significantly reduced the intracellular ROS content in macrophages (Figure 2d-e), suggesting that the VIP in VPZG exhibited an antioxidative stress effect on macrophages. Moreover, flow cytometry analysis further confirmed that VPZG exhibited ROS scavenging properties (Figure 2f). We also analyzed the mRNA expression levels of proinflammatory factors (interleukin 1-beta [*IL-1β*] and *IL-6*) and anti-inflammatory factors (*IL-4* and *IL-10*) in each group using qPCR. Compared to that of the control group, the expression of *IL-1β* and *IL-6* was significantly downregulated after VPZG treatment, reaching levels comparable to those of the blank group. In contrast, VPZG significantly upregulated the expression of *IL-4* and *IL-10* compared to that in the control group (Figure 2g). This result indicates that VPZG regulates the secretion of inflammatory factors in macrophages. Collectively, these findings indicate that VPZG promotes macrophage M2 polarization, reduces intracellular ROS levels, and regulates the expression of inflammatory factors.

VPZG Regulates Macrophage Repolarization via the NF-κB Signaling Pathway. To investigate the effect of VPZG on macrophages, we performed mRNA transcriptome sequencing to evaluate the regulation of macrophage polarization homeostasis by VPZG at the gene level. The differential gene volcano plot revealed 313 upregulated genes and 273 downregulated genes after treatment with VPZG compared to those in the control group (Figure S4). Gene Ontology enrichment analysis indicated that in macrophages treated with VPZG, the inflammatory response, chemokine activity, and chemokine receptor binding activity were all downregulated (Figure 3a and S5). Kyoto Encyclopedia of Genes and Genomes (KEGG) enrichment analysis demonstrated that the NF-κB, tumor necrosis factor-alpha (TNF-α), and IL-17 pathways were significantly downregulated in macrophages after treatment with VPZG (Figure 3b-e). These results indicate that VPZG regulates macrophage polarization homeostasis mainly by downregulating the core molecules of the inflammation-activated NF-κB, TNF, and IL-17 signaling pathways. This downregulation, in turn, reduces the secretion and release of macrophage inflammatory factors, thus

https://doi.org/10.1021/acsnano.4c16917
ACS Nano 2025, 19, 13871−13888

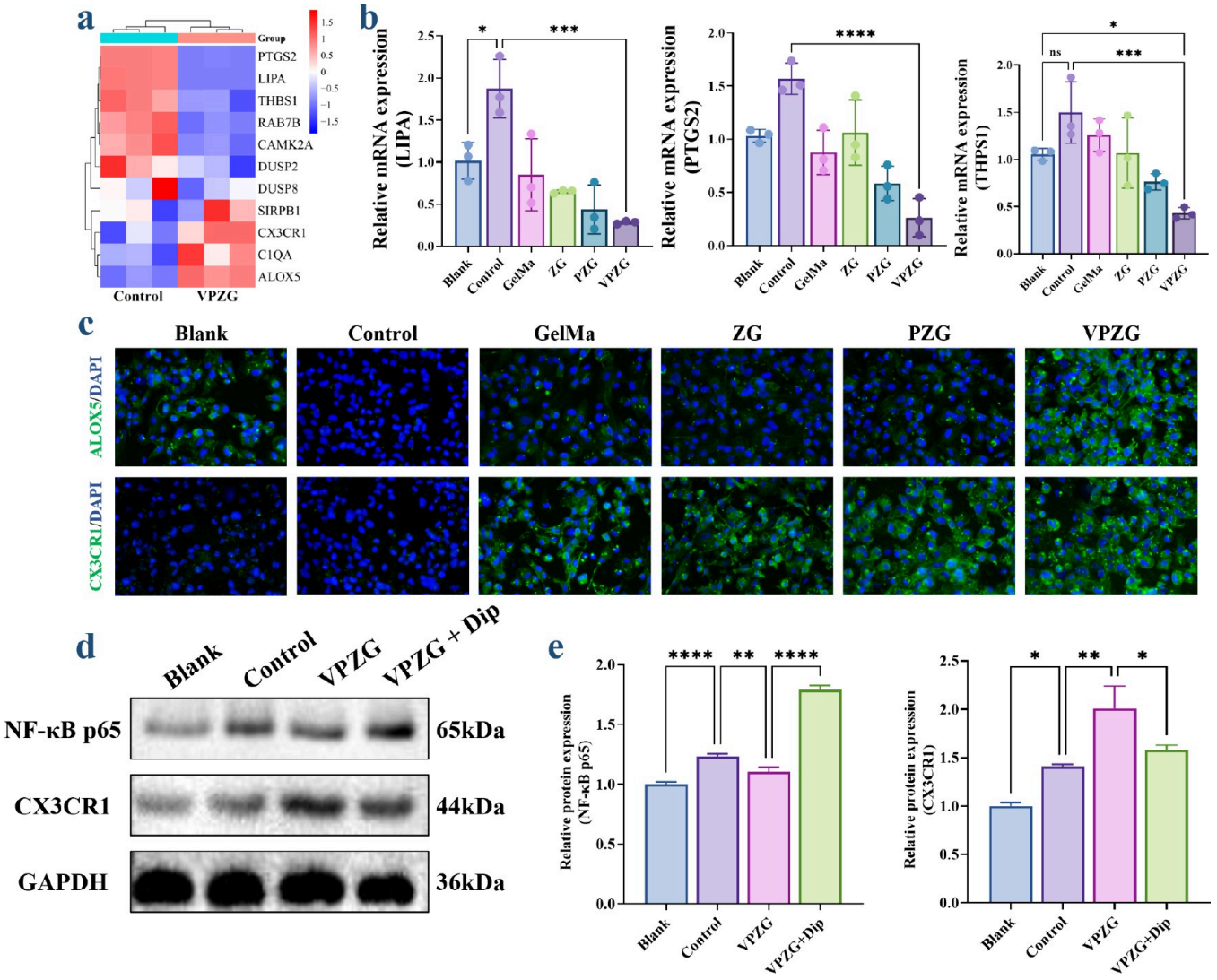

Figure 4. VPZG Induces Efferocytosis of Macrophages*In Vitro*. (a) Heatmap of the differences in the expression of genes related to the efferocytosis effect in THP-1 cells between the control and VPZG groups. (b) qPCR analysis of the relative changes in mRNA expression levels of genes related to efferocytosis in THP-1 cells (b). (c) Immunofluorescence analysis of protein expression in each group. (d) Changes in the expression of the efferocytosis-related protein CX3CR1 after treatment with the NF-κB pathway agonist Diprovocim (abbreviated as Dip). (e) Semiquantitative analysis of protein expression. *$p < 0.05$, **$p < 0.01$, ***$p < 0.001$, ****$p < 0.0001$. Expressed as mean ± SEM. VPZ, VIP@PLGA@ZIF-8@GelMa; GelMa-loaded VIP@PLGA@ZIF-8; VPZG, VPZ nanoparticle; GelMa, LPS + GelMa added; ZG, with LPS+ZIF-8@GelMa added; PZG, with LPS+PLGA@ZIF-8@GelMa; and VPZG, with LPS+VIP@PLGA@ZIF-8@GelMa added.

promoting macrophage M2 polarization. Western blotting further verified the VPZG-induced decreases in the expression of NF-κB p65 and the inflammatory markers IL-17, TNF-α, and IL-1β compared to those in the control group (Figure 3f–g). Collectively, these results indicate that VPZG may regulate polarization homeostasis by downregulating the expression of macrophage inflammatory factors through the NF-κB signaling pathway.

VPZG Induces Efferocytosis of Macrophages *In Vitro*. Efferocytosis is the process of clearing apoptotic cells, which are dead or nonfunctional. It plays a key role in the maintenance of tissue homeostasis, promotion of tissue regeneration, and immune regulation.[25,26] Our KEGG results revealed significant changes in cellular processes related to efferocytosis. Therefore, we further analyzed the changes in macrophage efferocytosis-related gene expression after treatment with VPZG. The differential gene heatmap is presented in Figure 4a. The mRNA expression levels of efferocytosis-related genes and the mRNA expression of *LIPA*, *PTGS2*, and *THBS1* were significantly downregulated in the VPZG group compared to those in the control group (Figure 4b). Immunofluorescence assays revealed increased CX3CR1 and ALOX5 protein expression in the VPZG treatment group compared to those in the control group (Figure 4c).

As the NF-κB pathway is related to cellular efferocytosis,[27,28] we hypothesized that VPZG could regulate cellular efferocytosis by downregulating this pathway. Our results indicated that VPZG downregulated NF-κB p65 expression but upregulated CX3CR1 expression. Notably, these effects were inhibited by treatment with Diprovocim, an NF-κB agonist (Figure 4d-e). These results suggest that VPZG may promote efferocytosis in macrophages by downregulating NF-κB p65 expression. As tendon injury repair involves the recruitment of TSPCs by macrophages, which help regulate local tissue inflammation, further investigation is needed to explore the role of VPZG in stem cell regulation during this process.

https://doi.org/10.1021/acsnano.4c16917
ACS Nano 2025, 19, 13871−13888

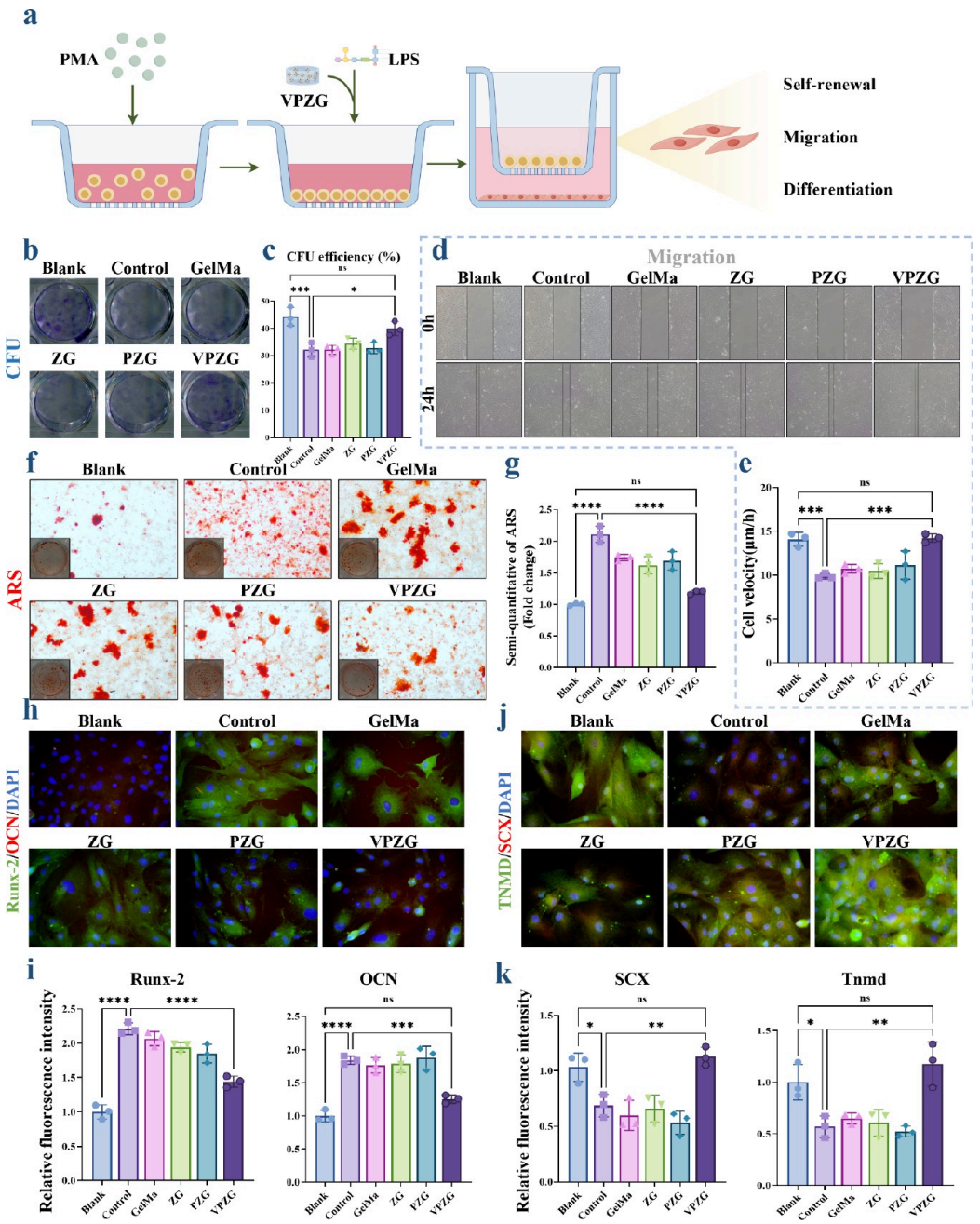

Figure 5. VPZG Enhances the Functionality of TSPCs*in vitro*by Modulating Immune Homeostasis. (a) Coculture pattern diagram of different groups of THP-1 cells with TSPCs. The fate of different Groups of TSPCs, such as (b) Crystal violet staining and (c) semiquantitative analysis, (d) Cell scratch assay with (e) semiquantitative analysis, (f) ARS staining and (g) semiquantitative analysis, (h) Immunofluorescence staining, and (i) semiquantitative analysis of osteogenesis-related genes (*Runx-2* and *Ocn*) and (j) immunofluorescence staining and (k) semiquantitative analysis of tenogenic-related genes (*Tnmd* and *Scx*). *$p < 0.05$, **$p < 0.01$, ***$p < 0.001$, ****$p < 0.0001$, ns: no significance. Expressed as mean ± SEM. VPZ, VIP@PLGA@ZIF-8@GelMa; GelMa-loaded VIP@PLGA@ZIF-8; VPZG, VPZ nanoparticle; GelMa, LPS + GelMa added; ZG, with LPS+ZIF-8@GelMa added; PZG, with LPS+PLGA@ZIF-8@GelMa; and VPZG, with LPS+VIP@PLGA@ZIF-8@GelMa added.

VPZG Enhances the Functionality of TSPCs *In Vitro* by Modulating Immune Homeostasis. We used LPS-induced macrophages to mimic the local inflammatory microenvironment. We then cocultured each group of induced macrophages with TSPCs to explore the effect of VPZG on the fate of TSPCs through the modulation of macrophage polarization (Figure 5a). The colony-forming unit (CFU) assay verified the clonogenic capacity of stem cells. Compared with the normal blank group, the clonogenic capacity of TSPCs in the control group was reduced, which was improved by treatment with VPZG (Figure 5b-c). Additionally, the migratory capacity of TSPCs plays an important role in tissue injury repair. In the inflammatory microenvironment (control group), the migratory ability of TSPCs was impaired, whereas it was significantly improved in the VPZG group (Figure 5d-e). As presented in Figure S6, VPZG increased the protein expression of Oct4, a stemness marker for TSPCs, compared to that in the control group.

https://doi.org/10.1021/acsnano.4c16917
ACS Nano 2025, 19, 13871−13888

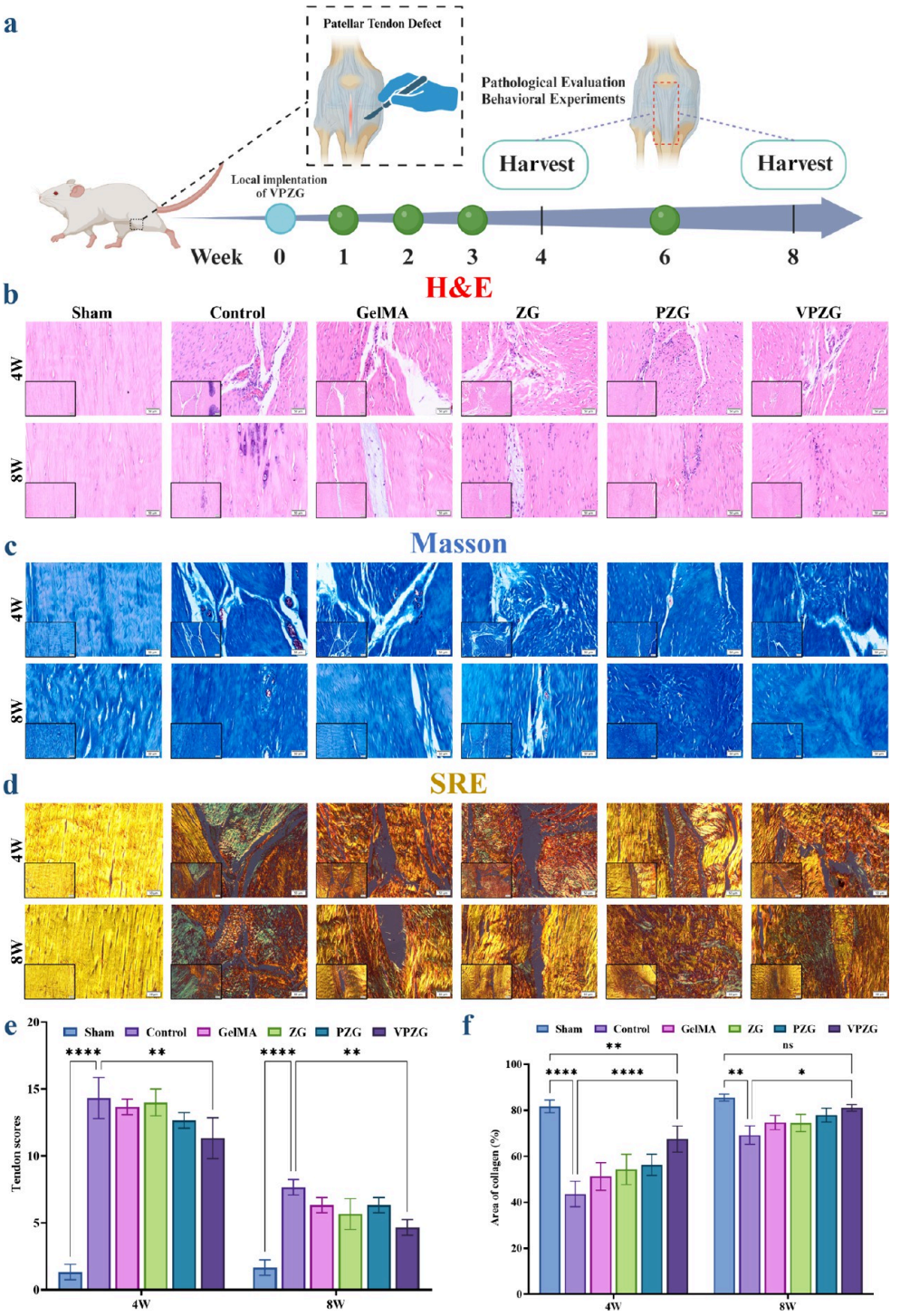

Figure 6. VPZG Promotes Patellar Tendon Repair in SD Rats. (a) Schematic illustration of the establishment of a rat patellar tendon defect model and a flowchart of VPZG implantation. Pathological evaluation at 4 and 8 weeks postoperatively: (b) Hematoxylin and eosin staining, (c) Masson staining, and (d) Sirius staining of rat patellar tendon in different treatment groups. (e) Tendon tissue scoring. (f) Semiquantitative analysis of collagen area. *$p < 0.05$, **$p < 0.01$, ****$p < 0.0001$, ns: no significance. VPZ, VIP@PLGA@ZIF-8@GelMa; GelMa-loaded VIP@PLGA@ZIF-8; VPZG, VPZ nanoparticle; GelMa, LPS + GelMa added; ZG, with LPS+ZIF-8@GelMa added; PZG, with LPS+PLGA@ZIF-8@GelMa; and VPZG, with LPS+VIP@PLGA@ZIF-8@GelMa added.

Furthermore, the imbalanced differentiation of TSPCs is a key factor contributing to the difficulty of repairing tendon injuries. Impaired TSPC function results in increased osteogenic differentiation and decreased tenogenic differentiation.[6] Therefore, we examined the multilineage differentiation ability of TSPCs. Compared to that in the control group, the number of alizarin red-stained calcium nodules was decreased in the VPZG group (Figure 5f–g). Immunofluorescence analysis revealed a decrease in the protein expression of osteogenesis-related genes (*Runx2* and *Ocn*) (Figure 5h-i), indicating a decreased osteogenic ability of TSPC following treatment with VPZG. Additionally, the protein expression

https://doi.org/10.1021/acsnano.4c16917
ACS Nano 2025, 19, 13871−13888

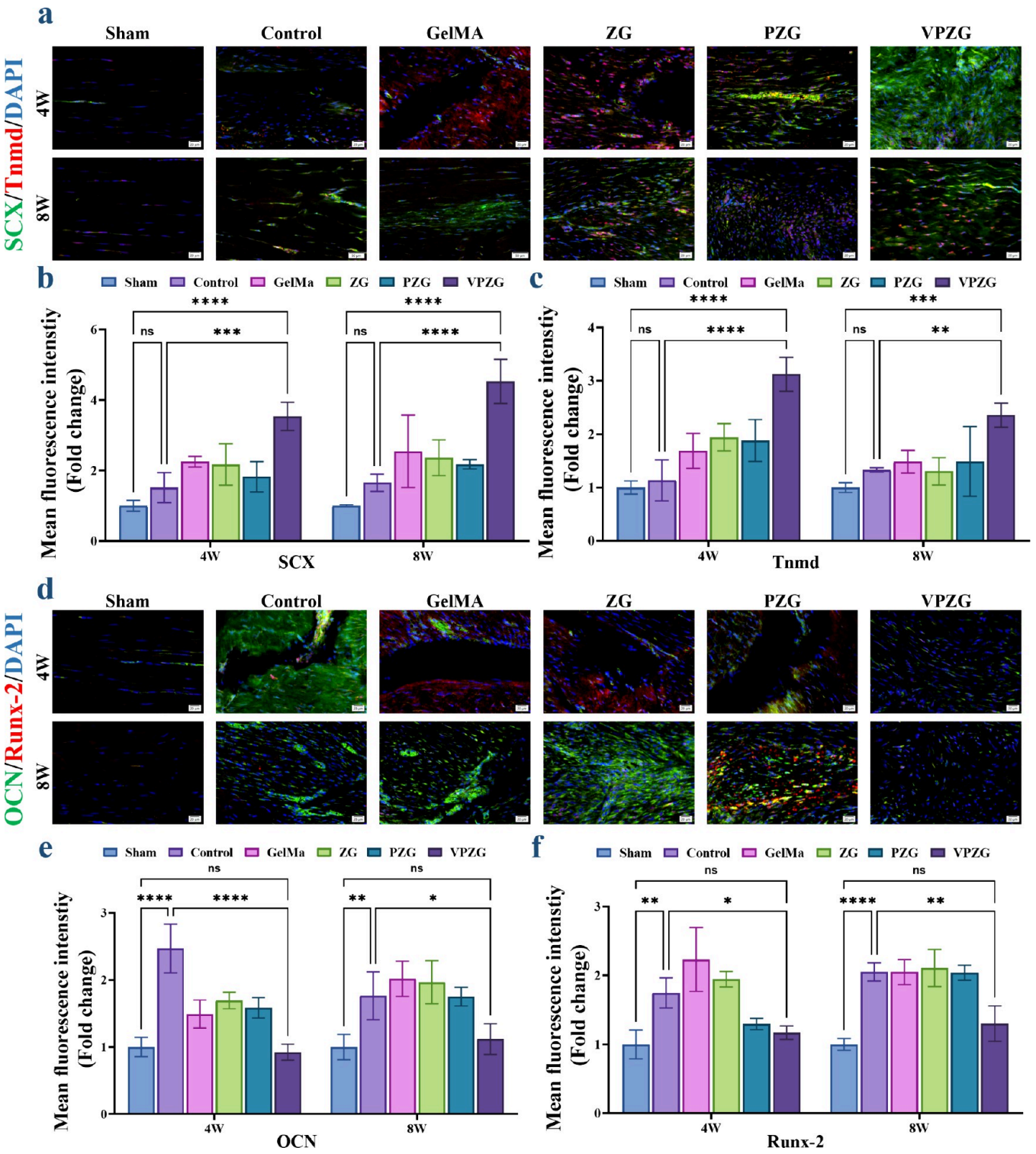

Figure 7. VPZG Upregulates the Expression of Tenogenic-related Markers in the Injury Site of the Patellar Tendon. (a) Immunofluorescence staining targeting tenogenic-related markers (TNMD and SCX). (b, c) Semiquantitative analysis of the immunofluorescence results. (d) Immunofluorescence staining for osteogenic-related markers (RUNX2 and OCN). (e, f) Semiquantitative analysis of the results. *$p < 0.05$, **$p < 0.01$, ***$p < 0.001$, ****$p < 0.0001$, ns: no significance. VPZ, VIP@PLGA@ZIF-8@GelMa; GelMa-loaded VIP@PLGA@ZIF-8; VPZG, VPZ nanoparticle; GelMa, LPS + GelMa added; ZG, with LPS+ZIF-8@GelMa added; PZG, with LPS+PLGA@ZIF-8@GelMa; and VPZG, with LPS+VIP@PLGA@ZIF-8@GelMa added.

levels of tenogenic-related genes (*Tnmd* and *Scx*) in TSPCs were also higher in the VPZG group than in the control group (Figure 5j-k), indicating that VPZG improved the tenogenic differentiation ability of TSPCs. These results indicate that VPZG improves the function of TSPCs by regulating macrophage polarization and reducing the expression of inflammatory factors in the stem cell niche, which is the basis for promoting tendon injury repair.

https://doi.org/10.1021/acsnano.4c16917
ACS Nano 2025, 19, 13871−13888

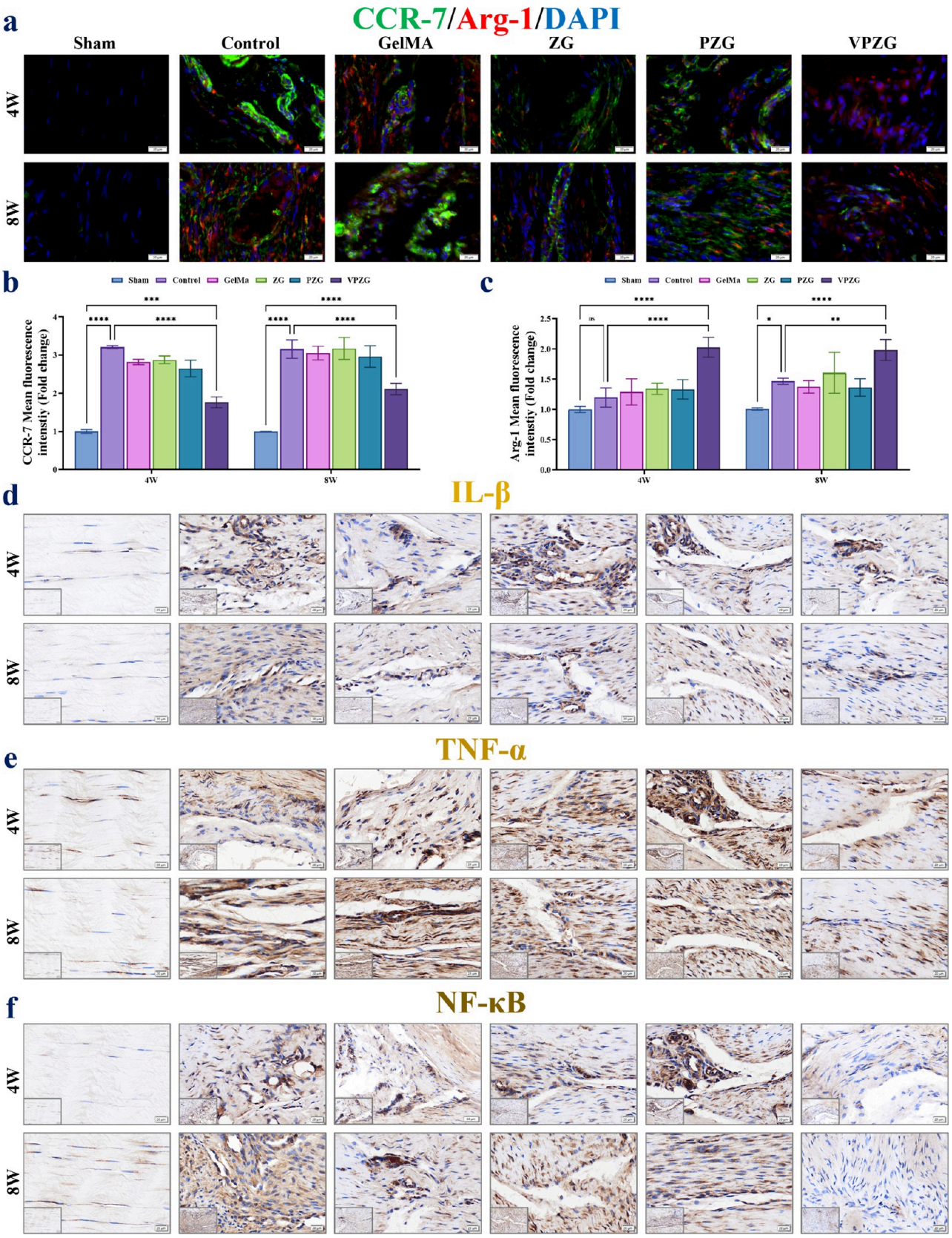

Figure 8. VPZG Enhances Tendon Regeneration*In Vivo*by Facilitating M2 Polarization of Macrophage and Reducing the Levels of Inflammatory Factors. (a) Immunofluorescence staining and (b, c) semiquantitative analysis of the M1 marker CCR-7 and M2 marker Arg-1 around the patellar tendon injury site at 4 versus 8 weeks postoperatively. Immunohistochemical staining for (d) IL-1β, (e) TNF-α, and (f) NF-κB. *$p < 0.05$, **$p < 0.01$, ***$p < 0.001$, ****$p < 0.0001$.VPZ, VIP@PLGA@ZIF-8@GelMa; GelMa-loaded VIP@PLGA@ZIF-8; VPZG, VPZ nanoparticle; GelMa, LPS + GelMa added; ZG, with LPS+ZIF-8@GelMa added; PZG, with LPS+PLGA@ZIF-8@GelMa; and VPZG, with LPS+VIP@PLGA@ZIF-8@GelMa added; IL-1β, interleukin 1-beta; TNF-α, tumor necrosis factor-alpha.

https://doi.org/10.1021/acsnano.4c16917
ACS Nano 2025, 19, 13871−13888

VPZG Promotes Patellar Tendon Repair in SD Rats. To further verify that VPZG exhibited a potent therapeutic effect on tendon tissue injury, we partially resected the patellar tendon of 8-week-old rats according to the method described in an earlier study.[23] We then implanted various types of hydrogels into the patellar tendon defect (Figure 6a). We first demonstrated the biosafety of the hydrogels in each group. To this end, we collected the heart, liver, spleen, lungs, and kidneys from each group at 4 and 8 weeks postoperatively for histological evaluation (Figure S7−8). We observed no significant impairment of vital organs caused by the hydrogel implantation in each group compared to the sham-operated group. Hematoxylin and eosin staining of patellar tendon tissue (Figure 6b) demonstrated that compared to the control group, local injection of VPZG reduced angiogenesis, inflammatory cell infiltration, and collagen misalignment at 4 weeks postoperatively. At 8 weeks, the VPZG group exhibited superior healing, with reduced deposition of vesicle-like structures in the cartilage matrix and well-aligned histiocytes. Compared to the control group, treatment with VPZG led to reduced tendon tissue scores at 4 and 8 weeks postoperatively, demonstrating its potential for tissue repair-promoting effect.

We further evaluated collagen formation and type using Masson and Sirius red staining (Figure 6c-d). VPZG promoted the restoration of aligned collagen structures compared to that in the control group. A semiquantitative analysis of collagen at the injury site revealed that the VPZG group exhibited increased collagen formation at 4 and 8 weeks postoperatively compared to the control group (Figure 6f), with a predominance of type I and type III collagen alignment. Immunofluorescence experiments indicated that the expression of local tendon-related markers TNMD and SCX was higher in the implanted VPZG at 4 and 8 weeks than in the control group (Figure 7a−c). This result highlights the superior therapeutic effect of VPZG. Additionally, we assessed the expression of the injury site osteogenesis-related markers OCN and RUNX-2 (Figure 7d-f). The VPZG group exhibited lower expression levels of OCN and RUNX-2 at 4 and 8 weeks postoperatively than those of the control group. These results suggest that VPZG promotes healing of patellar tendon injury by enhancing the tenogenic capacity of local stem cells. Overall, the histopathological analysis confirmed the biosafety of VPZG and its function in promoting tendon injury regeneration.

VPZG Enhances Tendon Regeneration *In Vivo* by Facilitating M2 Polarization of Macrophage and Reducing the Levels of Inflammatory Factors. We then sought to elucidate the mechanism by which VPZG specifically promotes tendon injury repair *in vivo*. To assess the distribution of different types of macrophages, we performed immunofluorescence analysis of CCR7 and Arg-1 expression around the injury site in each group (Figure 8a−c). The results revealed an increase in the number of CCR-7-positive cells in the control group compared to that in the sham-operated group. The number of Arg-1-positive cells around the injury site also increased 4 weeks after treatment with VPZG. Moreover, the percentage of CCR-7-positive cells decreased while that of Arg-1-positive cells increased in the VPZG group compared to those in the control group at 8 weeks postoperatively. This result suggests that in the early stages of patellar tendon injury, VPZG promotes M2 polarization of macrophages recruited to the injury site via the slow release of VIP.

Additionally, we performed immunohistochemical staining for key factors identified in RNA-Seq and Western blotting *in vitro*. The results demonstrated elevated expression of proinflammatory factors IL-1β and TNF-α in tendon tissues following injury (Figure 8d−f). Notably, topical application of VPZG reduced the expression of these proinflammatory factors. As our *in vitro* experiments demonstrated that VPZG promotes macrophage M2 polarization by decreasing NF-κB expression, we investigated whether the same effect is observed *in vivo*. Immunohistochemical analysis revealed increased NF-κB expression around the local injury site following injury. However, treatment with VPZG significantly downregulated NF-κB expression at 4 weeks compared to that at 8 weeks. These results suggest that VPZG exhibits a strong inhibitory effect on the inflammatory activation caused by tendon injury, which supports tendon injury repair and helps inhibit tendinopathy.

DISCUSSION

Tendon injuries are common and affect the quality of life of the patients. The pathological process of tendon self-repair includes the inflammatory, proliferative, and remodeling phases.[29] In the early stages of tendon injury, the formation of a localized inflammatory microenvironment promotes the activation and recruitment of immune cells and stem cells, which is a typical bodily response to injury.[30] However, persistent excessive inflammation disrupts collagen and cellular metabolism within the tendon tissue. This disruption subsequently impairs the endogenous repair function of the tendon, complicating tendon repair and tendinopathy.[31,32] As a result, natural homeostasis between proinflammatory M1 and anti-inflammatory M2 phenotypes emerges within the inflammatory microenvironment. Therefore, identifying and developing strategies targeting macrophage polarization could serve as a potential immune modulation approach, shifting the immune response toward a regenerative state for tendon repair. Notably, exogenous supplementation of bioactive peptides and proteins plays a crucial role in rotator cuff injury repair. For example, BMP-12 promotes tendon function recovery while demonstrating good feasibility and safety.[33] Furthermore, recombinant POSTN can enhance the proliferation and tenogenic differentiation of TSPCs, facilitating the healing of complete Achilles tendon injuries.[34] Based on these data, we designed VIP-loaded nanoparticles and implanted them at the site of tendon injury in rats to promote tendon repair. VPZG facilitated tendon injury repair by regulating immune homeostasis and enhancing TSPCs function. Our findings suggest that VPZG is a promising avenue for the clinical improvement of tendon injury treatment. Specifically, VPZG exhibited superior anti-inflammatory effects *in vitro*, promoting macrophage M2 polarization and reducing the expression of macrophage proinflammatory factors. Mechanistically, our results indicate that VPZG modulates immune homeostasis through the slow-release VIP-mediated NF-κB signaling pathway to promote macrophage efferocytosis. Given the important role of TSPCs in tendon injury repair, we simultaneously treated macrophages and TSPCs with VPZG. Our results indicate that VPZG enhances stem cell cloning, migration, and tendon formation. Moreover, local implantation of VPZG into rat patellar tendon injury sites exhibited a good safety profile *in vivo*. At 4 and 8 weeks after implantation, VPZG promoted the M2 polarization of macrophages at the injury site and decreased the expression levels of proin-

https://doi.org/10.1021/acsnano.4c16917
ACS Nano 2025, 19, 13871−13888

flammatory factors in the damaged tendon tissue. At the cellular and tissue levels, VPZG promoted the expression of tenogenic genes around the tendon injury site. Overall, these findings indicate that VPZG promotes tendon injury repair by targeting immune homeostasis to reduce the expression of inflammatory factors and enhance stem cell function.

We designed PLGA@ZIF-8 loaded VIP to form slow-release nanoparticles, aiming to enhance the localized sustained slow release of VIP. We used GelMA to create hydrogels that facilitate implantation at tendon injury sites. PLGA is widely used in the biomedical field owing to its good biocompatibility and biodegradability.[35] It gradually degrades in the body and releases drugs without causing significant toxicity.[36,37] ZIF-8 (Zeolitic imidazolate framework-8), a commonly used metal−organic framework, offers several advantages. These include a high drug-loading capacity, pH-responsive release, biocompatibility, and multifunctional adaptability of ZIF-8, making it an excellent drug delivery platform for tendon repair.[38,39] Combined with the properties of PLGA, the drug-loading capacity of ZIF-8 can be improved,[40] resulting in an increased drug encapsulation in nanomaterials. Our VPZG system leverages these advantages to overcome the limitations of conventional systems. It offers a targeted, sustained, and inflammation-responsive therapeutic strategy tailored to meet the dynamic requirements of tendon regenerative medicine. Our study significantly advances the understanding of the role of VIP in tendon repair by demonstrating its dual functionality in immune modulation and stem cell enhancement. This distinguishes it from previous research focusing on singular aspects of the regenerative potential of VIP. For example, VIP has been demonstrated to promote M2 macrophage polarization in alveolar bone healing[41] and regulate intestinal homeostasis via epithelial progenitor cell modulation.[42] However, our study uniquely highlights its ability to enhance the tenogenic differentiation of TSPCs alongside immune regulation, offering a more comprehensive therapeutic strategy. Furthermore, our VPZG nanoparticle system, which integrates precise targeting and sustained-release properties, represents a novel approach compared to previous studies utilizing single growth factors, such as TGF-β-loaded PLGA-b-PEG nanoparticles for tendon repair.[43] Our findings also build on the established role of M2 macrophage polarization in tendon healing[44] by demonstrating that VIP further downregulates the NF-κB axis to enhance anti-inflammatory effects. Moreover, our coculture system, which mimics the *in vivo* microenvironment, represents an advancement over previous methods that relied solely on mechanical or biochemical stimulation, such as direct treatment of TSPCs with growth factors and ascorbic acid.[45] By combining immune modulation and stem cell activation, our VPZG-based approach addresses multiple aspects of tendon healing. This also distinguishes it from prior research focused on single therapeutic targets and underscores its significance in the broader context of regenerative medicine.

Macrophages, which play an important role in immune homeostasis and inflammatory regulation, polarize into M1-polarized (proinflammatory) and M2-polarized (anti-inflammatory) phenotypes. M2 macrophages facilitate tissue repair. For example, Milica et al. induced macrophage M2 polarization using a hydrogel-loaded angiopoietin-1 mimetic peptide, which effectively promoted wound healing.[46] Yang et al.[47] suggested that promoting macrophage M2 polarization to regulate immune homeostasis could prevent tendon heterotopic ossification. While M2 macrophages play a beneficial role in tissue regeneration by promoting anti-inflammatory responses and enhancing tissue repair, an excessive or prolonged M2 polarization could potentially lead to fibrosis.[48,49] This could lead to the deposition of excessive extracellular matrix components, including collagen, potentially impairing the normal architecture and function of the tendon. We emphasize that, while M2 polarization is beneficial in the early stages of healing, it is essential for the immune response to transition back to a balanced state to avoid the risk of pathological fibrosis.[50] In tendon repair, this balance is crucial to ensure that collagen deposition supports the proper structural alignment and mechanical properties of the tendon, rather than causing scarring or impaired tissue function.[13,51,52] Macrophage efferocytosis, the process of phagocytosing apoptotic cells,[53] facilitates the clearance of inflammatory factor-induced apoptotic cells. Lee et al. proposed that enhanced macrophage efferocytosis reduces the level of inflammation, preventing cardiovascular diseases.[4] Additionally, chronic inflammation or tissue damage can lead to the excessive activation of the NF-κB axis, exacerbating the progression of tendinopathy and hindering tendon repair.[54] Mechanistically, NF-κB serves as a critical regulator of macrophage polarization, with its activation promoting the proinflammatory M1 phenotype.[55] However, its overactivation can result in inflammatory infiltration, which, in turn, disrupts stem cell function and diminishes the endogenous repair capacity of the tissue. Therefore, the balance between macrophage polarization and immune homeostasis mediated by efferocytosis is crucial for tissue repair. In the present study, we established a rat patellar tendon injury model and used VIP-loaded VPEG. This system effectively promoted tendon injury repair capacity by inducing macrophage M2 polarization. It also enhanced macrophage efferocytosis to clear inflammatory apoptotic cells and regulates immune homeostasis at the site of tendon injury by inhibiting. NF-κB activity. VPEG targeted the inflammatory microenvironment by reducing inflammatory factor (TNF-α and IL-1β) secretion. It also restored the cellular dysfunction of inflammation-induced TSPCs, facilitating tendon repair.

Increasing evidence suggests that the nervous system plays an active role in regulating pain, inflammation, and tissue repair through the secretion of neurotransmitters.[56,57] In a rat model of Achilles tendon injury, axon germination and growth during tendon healing are correlated with neuropeptides in a time-dependent manner.[58] VIP is a neurotransmitter with vasodilatory and immunomodulatory properties expressed in many organs, including the central nervous system, lungs, and bone tissue.[59] VIP can inhibit the release of proinflammatory cytokines, such as IL-1 and TNF, by binding to VIP receptors on tissue macrophages.[60] Notably, a previous clinical trial on the use of aviptadil (a vasoactive intestinal polypeptide analog) for treating COVID-19 demonstrated significant improvements in oxygenation and survival rates in patients, along with a significant decrease in cytokine IL-6 *in vivo* after 60 days of drug use.[61] Moreover, inadequate VIP levels in intestinal tissues can lead to decreased *IL-10* mRNA expression, resulting in intestinal regulatory B cell dysfunction and inflammatory bowel disease. However, VIP supplementation can restore the dynamic balance of intestinal immunity and prevent the development of the disease.[62] Furthermore, VIP effectively inhibits NF-κB phosphorylation and reduces the expression of TNF-α and IL-17 in macrophages after inflammation induction, thus attenuating LPS-induced acute lung injury.[63]

https://doi.org/10.1021/acsnano.4c16917
ACS Nano 2025, 19, 13871−13888

VIP can also enhance osteogenesis and support bone repair by modulating the inflammatory response and promoting angiogenesis.[21] Similarly, in nerve tissue, VIP contributes to nerve regeneration by promoting neuroprotection, reducing inflammation, and stimulating nerve growth factor secretion.[64,65] Therefore, the ability of VIP to regulate macrophage polarization, promote anti-inflammatory responses, and enhance stem cell function appears to be consistent across these tissues.[66] Our findings are consistent with studies suggesting that VIP exerts significant anti-inflammatory effects *in vivo*. Our results also indicate that VPZG reduces the expression of proinflammatory factors (IL-1β, IL-17, TNF-α) in the local inflammatory microenvironment through the slow release of VIP, promoting macrophage M2 polarization and enhancing macrophage efferocytosis. *In vitro*, VPZG maintained the expression of Oct-4, a key stemness factor in TSPCs, and enhanced stem cell functions, such as cloning, migration, and tendon formation. Overall, these findings highlight the anti-inflammatory effects of VIP. Nevertheless, the specific outcomes and mechanisms may vary depending on the tissue type and injury context.

The sustained release of VIP via VPZG nanoparticles represents a promising therapeutic approach for tendon repair. By addressing key challenges in tendon healing, this strategy has the potential to significantly improve clinical outcomes, such as targeted and sustained delivery, immune modulation, and enhanced stem cell function. However, future research should focus on optimizing nanoparticle formulation, validating efficacy in larger animal models, and conducting clinical trials to translate this innovative treatment for patient use. Although our study highlights the therapeutic potential of the VIP-loaded VPZG for tendon repair, it is critical to recognize certain limitations. Despite being a well-established model, the rat patellar tendon injury model does not reflect clinical scenarios; therefore, our findings must be validated in a larger animal model. Second, we used macrophages cocultured with TSPCs to observe the stem cell phenotype; however, this approach lacked further mechanistic investigation. Therefore, additional mechanistic investigations of intercellular communication are warranted.

CONCLUSIONS

In conclusion, we demonstrated the positive effect of VPZG, an anti-inflammatory biomaterial, on the repair of patellar tendon injury in a rat model. VPZG regulates immune homeostasis around the injury site by reducing the expression levels of inflammatory factors through the NF-κB signaling pathway, promoting M2 polarization of macrophages and efferocytosis. VPZG also promotes tendon injury repair by enhancing the function of TSPCs. Therefore, VPZG has promising applications in tissue regeneration. Our VPZG system overcomes the limitations of conventional systems and offers a targeted, sustained, and inflammation-responsive therapeutic strategy for tendon regenerative medicine. However, further research is required to optimize nanoparticle formulation and validate its efficacy in larger animal models before its application in clinical trials.

MATERIALS AND METHODS

Synthesis and Characterization of VPZ. A total of 1 mg of VIP protein was dissolved in 1 mL of ethanol and sonicated for 5 min to ensure uniform dissolution in ethanol. Subsequently, 1 mg of ZIF8 was added, and sonication continued for 10 min to achieve uniform dispersion of ZIF-8 in ethanol. The solution was shaken 6 h. The reacted solution was centrifuged at 10000 rpm for 10 min. The supernatant was then collected for testing, while the precipitate was lyophilized to obtain the ZIF-8 carrier protein sample. The raw material PLGA (100 mg) and Span 80 (500 μL) were evenly dissolved in 2.5 mL of dichloromethane, followed by the addition of 1 mg of VIP-loaded ZIF-8. The solution was sonicated for 10 min to ensure even dispersion, referred to as the inner oil phase solution.

To prepare the external aqueous phase solution, 0.2 g of PVA was weighed and homogeneously dissolved in 20 mL of pure water. In the first step, 200 μL of pure water was added to the inner oil phase solution, which was then sonicated at 720 W for 5 min (ice bath) to form a uniform colostrum. In the second step, the colostrum was added to the outer aqueous phase solution and sonicated at 720 W for 10 min (ice bath) to form a homogeneous complex emulsion. In the third step, the sonicated compound emulsion was transferred to a 50 mL beaker, magnets were added, and the mixture was stirred at 900 rpm overnight. Finally, the emulsion was centrifuged at 6000 rpm for 10 min, and the precipitate was collected as VPZ.

The morphology and particle size of the VPZ nanoparticles were observed using TEM (Netherlands) to characterize the VPZ nanoparticles. The size distribution and surface charge of elements, such as Zn, C, O, and N, in the VPZ nanoparticles were detected using zeta potential and nanoparticle size analyzer (Nano ZS90; Malvern Panalytical, Malvern, UK). The elemental composition, including the distribution and proportion of elements such as Zn, C, O, and N, in the VPZ nanoparticles was analyzed using energy spectrometry (JEM 2100F; JEOL Ltd., Tokyo, Japan). The crystal conformation of VPZ was analyzed using FTIR and X-ray diffraction (Netherlands).

Synthesis and Characterization of VPZG. For the synthesis of VPZG, VPZ nanoparticles were first added to different concentrations of GelMa (10, 15, and 20%) in sterile phosphate-buffered saline (PBS) and filtered through a 0.22 μm needle filter at room temperature. They were then irradiated with UV light for 5 min to form a Pue hydrogel system called VPZG, which was stored at 4 °C. Additionally, ZIF-8, PZ, and VPZ were added to GelMa for subsequent cellular and animal experiments.

For the characterization tests, the samples were lyophilized into powder form and examined separately using SEM. The rheological properties of the hydrogels were analyzed using a rheology analyzer, and material swelling was assessed. To determine the efficiency of VPZG I, the slow release of VIP, VPZG samples (in a rectangular shape) were soaked in 5 mL of PBS (pH = 7.4) and incubated at 37 °C. Samples were collected once on days 1, 3, 5, 7, 14, 21, 28, and 35. The concentration of VIP released from the samples was measured using the ELISA (Proteintech, China)method, and a drug release profile was constructed based on the measured concentrations.

Cultured of THP-1. All THP-1 cells were purchased from Beyotime (Jiangsu, China). Cells were cultured at 37 °C with 5% CO_2 in a complete medium containing 20% fetal bovine serum and 5% penicillin-streptomycin. When the cells reached 70−80% confluence, they were passaged, washed with PBS, digested with trypsin, resuspended, and transferred to new culture dishes. Cells were differentiated into macrophages using PMA. During culture, the medium was regularly changed (Every 3days).

Immunofluorescence. Cells were cultured and fixed with 4% paraformaldehyde under appropriate conditions, followed by washing with PBS to remove the fixative. The cells were then treated with a permeabilizing solution (0.1% Triton X-100) to enhance antibody penetration and washed again. A blocking solution (5% BSA) was then added to reduce nonspecific binding, followed by incubation and another wash with PBS. The cells were then incubated with the corresponding primary antibody for 12 h at 4 °C, followed by another wash. The cells were subsequently incubated with the fluorescently labeled secondary antibody for 2 h at 37 °C, followed by another wash. Finally, the fluorescent signals were observed and recorded using a fluorescence microscope to analyze the expression and distribution of the target protein.

https://doi.org/10.1021/acsnano.4c16917
ACS Nano 2025, 19, 13871−13888

ROS Assay. After cell culture, cells were treated with the ROS probe DCFH-DA and incubated at 37 °C for 20 min allow the probe to enter the cells and become activated. The cells were then washed with PBS to remove any unbound probes. ROS levels were quantified by detecting fluorescent signals inside the cells using flow cytometry or fluorescence microscopy. Finally, changes in intracellular ROS under different treatment conditions were assessed based on fluorescence intensity, followed by statistical analyses.

qPCR. RNA was extracted from the sample (Vazyme, China), and cDNA was synthesized using a reverse transcriptase enzyme. The qPCR system included a cDNA template, specific primers, fluorescent dyes (e.g., SYBR Green), and PCR buffer. The reaction system was transferred to a qPCR instrument(Vazyme, China), and the appropriate amplification cycle program was set. During the reaction, the fluorescence signal was monitored in real-time to quantify the expression level of the target gene. Finally, the relative expression was calculated by comparing the Ct values of the target genes to those of the internal reference genes in the samples, followed by statistical analysis.

Western Blot. Proteins were extracted from cell or tissue samples, and their concentrations were determined using the BCA or Bradford method. The samples were then heated, and the proteins were separated via SDS-PAGE electrophoresis. The separated proteins were then transferred to a PVDF or nitrocellulose membrane, which was then blocked with 5% skim milk powder or BSA, to prevent nonspecific binding. The membranes were then incubated with the corresponding primary antibody for 12h at 4 °C, followed by washing with a wash buffer. Subsequently, a secondary antibody (conjugated enzyme-labeled antibody) was added for 2 h at 37 °C, and the membranes were washed again. The signal was detected using a substrate chromogenic reaction, and the results were recorded using an imaging system. The expression level of the target protein was compared with that of the internal reference protein.

CFU. To assess the self-cloning ability of TSPCs, SD rat-derived TSPCs were obtained and the cell suspension was diluted to the appropriate concentration. The cells were then inoculated into Petri dishes containing appropriate medium and growth factors and then cultured for 7−10 days, allowing clear cell colonies to form. Subsequently, the number of CFUs was assessed by observing and counting the colonies under a microscope.

Migration Ability Assay. TSPCs were inoculated into 6-well plates until they reached 80−90% confluence. A sterile pipet was then used to gently create a straight scratch across the cell monolayer. The cells were then gently washed with the culture medium to remove detached cells. The plates were incubated for 24 h, and the healing of the scratched area was then photographed and observed under a microscope to assess cell migration. Finally, changes in the width of the scratches were measured using image analysis software (Olympus CKX53, China) to quantify the rate of cell migration and healing ability.

Osteogenic Differentiation. TSPCs were inoculated into 6-well plates and cultured to reach 80% confluence. The cells were then treated with an osteogenic induction medium to induce their differentiation into osteoblasts. The medium was changed periodically throughout the induction process. By day 14 of the culture, calcium deposits had formed in the TSPCs, which were subsequently stained using Alizarin red solution (Beyotime, China).

Tendon Defect Model. All animal experiments were approved by the Ethics Committee of the Medical School of Southeast University (approval no. 20230301023). Tendon defects were created in the patellar tendon of SD rats. To generate the tendon defect, a 1 mm portion of the central patellar tendon was excised from the tibial tuberosity to the tip of the patella. This was performed while avoiding damage to the fibrocartilaginous bands. This procedure was conducted using three stacked sharp blades, as previously described.[23] VPZG was also implanted into the defect site, and patellar tendon tissue samples were collected at 4 and 8 weeks postoperatively for subsequent experiments.

Histopathological Evaluation of Patellar Tendon. At the specified postoperative time points, patellar tendon tissue samples were harvested and fixed with 4% paraformaldehyde. The samples were then sectioned through paraffin embedding, and thin tissue sections were prepared. These tissue sections were subjected to routine histological staining (hematoxylin and eosin staining and Masson's staining) to observe tissue morphology. Immunohistochemical staining was conducted to detect the expression of specific proteins, utilizing appropriately labeled primary and secondary antibodies. Finally, immunofluorescence experiments were performed to observe the localization and expression of specific proteins using fluorescence microscopy.

Statistical Analysis. GraphPad Prism9 (GraphPad Inc., San Diego, CA, USA) was used for all statistical analyses. All experimental results are expressed as the mean value ± standard deviation (SD). Intergroup variability was assessed using a two-tailed Student's *t*-test for comparisons involving two groups or a one-way analysis of variance with Tukey's test comparison involving more than two groups.

ASSOCIATED CONTENT

Data Availability Statement

The data that support the findings of this study are available from the corresponding authors upon reasonable request.

Supporting Information

The Supporting Information is available free of charge at https://pubs.acs.org/doi/10.1021/acsnano.4c16917.

Primer sequence and antibody information used in the experiment (Supplementary Tables 1 and 2); characterization of VPZG, including zeta potential, appearance, encapsulation rate, and loading rate; biosafety experiments of VPZG, such as cytotoxic effects and impact on vital organs; transcriptomic analysis of VPZG-treated macrophages: volcano plots and GSEA of GO terms; WB of Oct-4 in the different TSPCs groups (Supporting Figures S1−S9) (PDF)

AUTHOR INFORMATION

Corresponding Authors

Yunfeng Rui − *Department of Orthopaedics, Zhongda Hospital, School of Medicine, Orthopaedic Trauma Institute, and Trauma Center, Zhongda Hospital, School of Medicine, Southeast University, Nanjing, Jiangsu 210009, PR China;* orcid.org/0000-0001-9019-5531; Email: ruiyunfeng@126.com

Liu Shi − *Department of Orthopaedics, Zhongda Hospital, School of Medicine, Orthopaedic Trauma Institute, and Trauma Center, Zhongda Hospital, School of Medicine, Southeast University, Nanjing, Jiangsu 210009, PR China;* orcid.org/0000-0002-8990-4019; Email: shiliu_gk@126.com

Authors

Hao Wang − *Department of Orthopaedics, Zhongda Hospital, School of Medicine, Orthopaedic Trauma Institute, and Trauma Center, Zhongda Hospital, School of Medicine, Southeast University, Nanjing, Jiangsu 210009, PR China*

Yucheng Gao − *Department of Orthopaedics, Zhongda Hospital, School of Medicine, Orthopaedic Trauma Institute, and Trauma Center, Zhongda Hospital, School of Medicine, Southeast University, Nanjing, Jiangsu 210009, PR China*

Jinyu Wang − *Department of Rehabilitation, Zhongda Hospital, School of Medicine, Southeast University, Nanjing, Jiangsu 210009, PR China*

Mumin Cao − *Department of Orthopaedics, Zhongda Hospital, School of Medicine, Orthopaedic Trauma Institute,*

https://doi.org/10.1021/acsnano.4c16917
ACS Nano 2025, 19, 13871−13888

and Trauma Center, Zhongda Hospital, School of Medicine, Southeast University, Nanjing, Jiangsu 210009, PR China

Guangchun Dai − *Department of Orthopaedics, Zhongda Hospital, School of Medicine, Orthopaedic Trauma Institute, and Trauma Center, Zhongda Hospital, School of Medicine, Southeast University, Nanjing, Jiangsu 210009, PR China*

Panpan Lu − *Department of Orthopaedics, Zhongda Hospital, School of Medicine, Orthopaedic Trauma Institute, and Trauma Center, Zhongda Hospital, School of Medicine, Southeast University, Nanjing, Jiangsu 210009, PR China*

Renwang Sheng − *Department of Orthopaedics, Zhongda Hospital, School of Medicine, Orthopaedic Trauma Institute, and Trauma Center, Zhongda Hospital, School of Medicine, Southeast University, Nanjing, Jiangsu 210009, PR China*

Cheng Zhang − *Department of Orthopaedics, Zhongda Hospital, School of Medicine, Orthopaedic Trauma Institute, and Trauma Center, Zhongda Hospital, School of Medicine, Southeast University, Nanjing, Jiangsu 210009, PR China*

Qianqian Wang − *Jiangsu Key Laboratory for Design and Manufacture of Micro-Nano Biomedical Instruments, School of Mechanical Engineering, Southeast University, Nanjing 210009, PR China;* orcid.org/0000-0001-8011-171X

Gang Li − *Institute of Biomedicine and Biotechnology Shenzhen Institute of Advanced Technology, Chinese Academy of Sciences, Shenzhen 518000, PR China*

Qi Yong H. Ai − *Department of Diagnostic Radiology, Faculty of Medicine, The University of Hong Kong, Hong Kong, SAR 999077, PR China*

Complete contact information is available at: https://pubs.acs.org/10.1021/acsnano.4c16917

Author Contributions

‡Hao Wang, Yu-Cheng Gao, and Jin-Yu Wang contributed equally to this work.

Author Contributions

The manuscript was written through contributions of all authors. All authors have given approval to the final version of the manuscript.

Funding

This work was supported by the National Natural Science Foundation of China (81871812 and 82201751), the Natural Science Foundation of Jiangsu Province (BK20221462), and the Fundamental Research Funds for the Central Universities [2242024RCB0055].

Notes

The authors declare no competing financial interest.

ABBREVIATIONS

VIP, Vasoactive intestinal peptide; TSPCs, Tendon stem/progenitor cells; VPZG, VIP@PLGA@ZIF-8@GelMa; SEM, Scanning electron microscopy; FTIR, Fourier-transform infrared; ELISA, Enzyme-linked immunosorbent assay; TEM, Transmission electron microscope; LPS, Lipopolysaccharide; DCFH-DA, 2′,7′-Dichlorofluorescin diacetate; ROS, Reactive oxygen species; IL, Interleukin; qPCR, Quantitative polymerase chain reaction; KEGG, Kyoto Encyclopedia of Genes and Genomes; TNF-α, Tumor necrosis factor-alpha; CFU, Colony-forming unit

REFERENCES

(1) Dai, G. C.; Wang, H.; Ming, Z.; Lu, P. P.; Li, Y. J.; Gao, Y. C.; Shi, L.; Cheng, Z.; Liu, X. Y.; Rui, Y. F. Heterotopic mineralization (ossification or calcification) in aged musculoskeletal soft tissues: A new candidate marker for aging. *Ageing Res. Rev.* **2024**, *95*, No. 102215.

(2) Chen, M.; Li, Y.; Xiao, L.; Dai, G.; Lu, P.; Rui, Y. Noncanonical Wnt5a signaling regulates tendon stem/progenitor cells senescence. *Stem Cell Res. Ther.* **2021**, *12* (1), 544.

(3) Dai, G.; Li, Y.; Zhang, M.; Lu, P.; Zhang, Y.; Wang, H.; Shi, L.; Cao, M.; Shen, R.; Rui, Y. The Regulation of the AMPK/mTOR Axis Mitigates Tendon Stem/Progenitor Cell Senescence and Delays Tendon Aging. *Stem Cell Rev. Rep* **2023**, *19* (5), 1492−1506.

(4) Lu, P.; Dai, G.; Shi, L.; Li, Y.; Zhang, M.; Wang, H.; Rui, Y.; Mussano, F. HMGB1Modulates High Glucose-Induced Erroneous Differentiation of Tendon Stem/Progenitor Cells through RAGE/beta-Catenin Pathway. *Stem Cells Int.* **2024**, *2024*, No. 2335270.

(5) Cao, M.; Sheng, R.; Sun, Y.; Cao, Y.; Wang, H.; Zhang, M.; Pu, Y.; Gao, Y.; Zhang, Y.; Lu, P.; Teng, G.; Wang, Q.; Rui, Y. Delivering Microrobots in the Musculoskeletal System. *Nanomicro Lett.* **2024**, *16* (1), 251.

(6) Wang, H.; Dai, G. C.; Li, Y. J.; Chen, M. H.; Lu, P. P.; Zhang, Y. W.; Zhang, M.; Cao, M. M.; Rui, Y. F. Targeting Senescent Tendon Stem/Progenitor Cells to Prevent or Treat Age-Related Tendon Disorders. *Stem Cell Rev. Rep* **2023**, *19* (3), 680−693.

(7) Zhang, M.; Wang, H.; Dai, G. C.; Lu, P. P.; Gao, Y. C.; Cao, M. M.; Li, Y. J.; Rui, Y. F. Injectable self-assembled GDF5-containing dipeptide hydrogels for enhanced tendon repair. *Mater. Today Bio* **2024**, *26*, No. 101046.

(8) Xu, H. T.; Lee, C. W.; Li, M. Y.; Wang, Y. F.; Yung, P. S.; Lee, O. K. The shift in macrophages polarisation after tendon injury: A systematic review. *J. Orthop Translat* **2020**, *21*, 24−34.

(9) He, Y.; Lu, S.; Chen, W.; Yang, L.; Li, F.; Zhou, P.; Chen, Z.; Wan, R.; Zhang, Z.; Sun, Y.; Lin, J.; Chen, Y.; Luo, Z.; Xu, C.; Chen, S. Exosomes derived from tendon stem/progenitor cells enhance tendon-bone interface healing after rotator cuff repair in a rat model. *Bioact Mater.* **2024**, *40*, 484−502.

(10) Sun, J.; Ju, F.; Jin, J.; Wang, H. L.; Li, Z. J.; Sun, Y. C.; Chen, Q. Z.; Yang, Q. Q.; Tan, J.; Zhou, Y. L. M2Macrophage Membrane-Mediated Biomimetic-Nanoparticle Carrying COX-siRNA Targeted Delivery for Prevention of Tendon Adhesions by Inhibiting Inflammation. *Small* **2023**, *19* (33), No. e2300326.

(11) Lui, P. P. Y.; Wong, C. M. Biology of Tendon Stem Cells and Tendon in Aging. *Front. Genet.* **2020**, *10*, 1338.

(12) Chen, B.; Zhao, X.; Xu, M.; Luo, J.; Bai, L.; Han, Q.; Gao, Y.; Guo, B.; Yin, Z. Inflammation-Responsive Functional Core-Shell Micro-Hydrogels Promote Rotator Cuff Tendon-To-Bone Healing by Recruiting MSCs and Immuno-Modulating Macrophages in Rats. *Adv. Healthcare Mater.* **2025**, *14* (2), No. e2404091.

(13) Zhang, X.; Song, W.; Liu, Y.; Han, K.; Wu, Y.; Cho, E.; Fang, Z.; Jiang, L.; Hu, Y.; Zhu, X.; Jiang, J.; Huangfu, X.; Zhao, J. Healthy Tendon Stem Cell-Derived Exosomes Promote Tendon-To-Bone Healing of Aged Chronic Rotator Cuff Tears by Breaking the Positive-Feedback Cross-Talk between Senescent Tendon Stem Cells and Macrophages through the Modulation of Macrophage Polarization. *Small* **2024**, *20* (31), No. e2311033.

(14) Ganea, D.; Hooper, K. M.; Kong, W. The neuropeptide vasoactive intestinal peptide: direct effects on immune cells and involvement in inflammatory and autoimmune diseases. *Acta Physiol (Oxf)* **2015**, *213* (2), 442−52.

(15) Guan, L.; Yu, D.; Wu, G. H.; Ning, H. J.; He, S. D.; Li, S. S.; Hu, T. Y.; Yang, G.; Liu, Z. Q.; Yu, H. Q.; Sun, X. Z.; Liu, Z. G.; Yang, P. C. Vasoactive intestinal peptide is required in the maintenance of immune regulatory competency of immune regulatory monocytes. *Clin. Exp. Immunol.* **2019**, *196* (2), 276−286.

(16) Castro-Vazquez, D.; Arribas-Castano, P.; Garcia-Lopez, I.; Gutierrez-Canas, I.; Perez-Garcia, S.; Lamana, A.; Villanueva-Romero, R.; Cabrera-Martin, A.; Tecza, K.; Martinez, C.; Juarranz, Y.; Gomariz, R. P.; Carrion, M. Vasoactive intestinal peptide exerts an osteoinductive effect in human mesenchymal stem cells. *Biofactors* **2024**, *50* (6), 1148−1160.

(17) Yelkenli, I. H.; Ulupinar, E.; Korkmaz, O. T.; Sener, E.; Kus, G.; Filiz, Z.; Tuncel, N. Modulation of Corpus Striatal Neurochemistry by Astrocytes and Vasoactive Intestinal Peptide (VIP) in Parkinsonian Rats. *J. Mol. Neurosci* **2016**, *59* (2), 280−9.
(18) Deng, G.; Jin, L. The effects of vasoactive intestinal peptide in neurodegenerative disorders. *Neurol Res.* **2017**, *39* (1), 65−72.
(19) Shi, L.; Wang, C.; Yan, Y.; Wang, G.; Zhang, J.; Feng, L.; Yang, X.; Li, G. Function study of vasoactive intestinal peptide on chick embryonic bone development. *Neuropeptides* **2020**, *83*, No. 102077.
(20) Shi, L.; Liu, Y.; Yang, Z.; Wu, T.; Lo, H. T.; Xu, J.; Zhang, J.; Lin, W.; Zhang, J.; Feng, L.; Li, G. Vasoactive Intestinal Peptide Promotes Fracture Healing in Sympathectomized Mice. *Calcif Tissue Int.* **2021**, *109* (1), 55−65.
(21) Shi, L.; Feng, L.; Zhu, M. L.; Yang, Z. M.; Wu, T. Y.; Xu, J.; Liu, Y.; Lin, W. P.; Lo, J. H. T.; Zhang, J. F.; Li, G. Vasoactive Intestinal Peptide Stimulates Bone Marrow-Mesenchymal Stem Cells Osteogenesis Differentiation by Activating Wnt/beta-Catenin Signaling Pathway and Promotes Rat Skull Defect Repair. *Stem Cells Dev* **2020**, *29* (10), 655−666.
(22) Gong, J.; Ye, C.; Ran, J.; Xiong, X.; Fang, X.; Zhou, X.; Yi, Y.; Lu, X.; Wang, J.; Xie, C.; Liu, J. Polydopamine-Mediated Immunomodulatory Patch for Diabetic Periodontal Tissue Regeneration Assisted by Metformin-ZIF System. *ACS Nano* **2023**, *17* (17), 16573−16586.
(23) Liu, Y.; Xu, J.; Xu, L.; Wu, T.; Sun, Y.; Lee, Y. W.; Wang, B.; Chan, H. C.; Jiang, X.; Zhang, J.; Li, G. Cystic fibrosis transmembrane conductance regulator mediates tenogenic differentiation of tendon-derived stem cells and tendon repair: accelerating tendon injury healing by intervening in its downstream signaling. *FASEB J.* **2017**, *31* (9), 3800−3815.
(24) Dou, Y.; Zhai, H.; Li, H.; Xing, H.; Zhu, C.; Xuan, Z. Endothelial cells-derived exosomes-based hydrogel improved tendinous repair via anti-inflammatory and tissue regeneration-promoting properties. *J. Nanobiotechnol.* **2024**, *22* (1), 401.
(25) Gerlach, B. D.; Ampomah, P. B.; Yurdagul, A., Jr.; Liu, C.; Lauring, M. C.; Wang, X.; Kasikara, C.; Kong, N.; Shi, J.; Tao, W.; Tabas, I. Efferocytosis induces macrophage proliferation to help resolve tissue injury. *Cell Metab* **2021**, *33* (12), 2445−2463e8.
(26) Geng, L.; Zhao, J.; Deng, Y.; Molano, I.; Xu, X.; Xu, L.; Ruiz, P.; Li, Q.; Feng, X.; Zhang, M.; Tan, W.; Kamen, D. L.; Bae, S. C.; Gilkeson, G. S.; Sun, L.; Tsao, B. P. Human SLE variant NCF1-R90H promotes kidney damage and murine lupus through enhanced Tfh2 responses induced by defective efferocytosis of macrophages. *Ann. Rheum Dis* **2022**, *81* (2), 255−267.
(27) Liu, S.; Wu, J.; Stolarz, A.; Zhang, H.; Boerma, M.; Byrum, S. D.; Rusch, N. J.; Ding, Z. PCSK9 attenuates efferocytosis in endothelial cells and promotes vascular aging. *Theranostics* **2023**, *13* (9), 2914−2929.
(28) An, Y.; Zhang, H.; Wang, C.; Jiao, F.; Xu, H.; Wang, X.; Luan, W.; Ma, F.; Ni, L.; Tang, X.; Liu, M.; Guo, W.; Yu, L. Activation of ROS/MAPKs/NF-kappaB/NLRP3 and inhibition of efferocytosis in osteoclast-mediated diabetic osteoporosis. *FASEB J.* **2019**, *33* (11), 12515−12527.
(29) Li, H.; Luo, S.; Wang, H.; Chen, Y.; Ding, M.; Lu, J.; Jiang, L.; Lyu, K.; Huang, S.; Shi, H.; Chen, H.; Li, S. The mechanisms and functions of TGF-beta1 in tendon healing. *Injury* **2023**, *54* (11), No. 111052.
(30) Hao, Z. W.; Zhang, Z. Y.; Wang, Z. P.; Wang, Y.; Chen, J. Y.; Chen, T. H.; Shi, G.; Li, H. K.; Wang, J. W.; Dong, M. C.; Hong, L.; Li, J. F. Bioactive peptides and proteins for tissue repair: microenvironment modulation, rational delivery, and clinical potential. *Mil. Med. Res.* **2024**, *11* (1), 75.
(31) Mishra, R.; Sehring, I.; Cederlund, M.; Mulaw, M.; Weidinger, G. NF-kappaB Signaling Negatively Regulates Osteoblast Dedifferentiation during Zebrafish Bone Regeneration. *Dev Cell* **2020**, *52* (2), 167−182e7.
(32) Sipp, D.; Robey, P. G.; Turner, L. Clear up this stem-cell mess. *Nature* **2018**, *561* (7724), 455−457.
(33) Ide, J.; Mochizuki, Y.; van Noort, A.; Ochi, H.; Sridharan, S.; Itoi, E.; Greiner, S. Local rhBMP-12 on an Absorbable Collagen Sponge as an Adjuvant Therapy for Rotator Cuff Repair-A Phase 1, Randomized, Standard of Care Control, Multicenter Study: Part 2-A Pilot Study of Functional Recovery and Structural Outcomes. *Orthop. J. Sports Med.* **2017**, *5* (9), 1994.
(34) Wang, Y.; Jin, S.; Luo, D.; He, D.; Shi, C.; Zhu, L.; Guan, B.; Li, Z.; Zhang, T.; Zhou, Y.; Wang, C. Y.; Liu, Y. Functional regeneration and repair of tendons using biomimetic scaffolds loaded with recombinant periostin. *Nat. Commun.* **2021**, *12* (1), 1293.
(35) Martins, C.; Sousa, F.; Araújo, F.; Sarmento, B. Functionalizing PLGA and PLGA Derivatives for Drug Delivery and Tissue Regeneration Applications. *Adv. Healthcare Mater.* **2018**, *7* (1), 1701035.
(36) Park, K.; Skidmore, S.; Hadar, J.; Garner, J.; Park, H.; Otte, A.; Soh, B. K.; Yoon, G.; Yu, D.; Yun, Y.; Lee, B. K.; Jiang, X.; Wang, Y. Injectable, long-acting PLGA formulations: Analyzing PLGA and understanding microparticle formation. *J. Controlled Release* **2019**, *304*, 125−134.
(37) Gu, B.; Sun, X.; Papadimitrakopoulos, F.; Burgess, D. J. Seeing is believing, PLGA microsphere degradation revealed in PLGA microsphere/PVA hydrogel composites. *J. Controlled Release* **2016**, *228*, 170−178.
(38) Xie, H.; Liu, X.; Huang, Z.; Xu, L.; Bai, R.; He, F.; Wang, M.; Han, L.; Bao, Z.; Wu, Y.; Xie, C.; Gong, Y. Nanoscale Zeolitic Imidazolate Framework (ZIF)-8 in Cancer Theranostics: Current Challenges and Prospects. *Cancers* **2022**, *14* (16), 3935.
(39) Poddar, A.; Conesa, J. J.; Liang, K.; Dhakal, S.; Reineck, P.; Bryant, G.; Pereiro, E.; Ricco, R.; Amenitsch, H.; Doonan, C.; Mulet, X.; Doherty, C. M.; Falcaro, P.; Shukla, R. Encapsulation, Visualization and Expression of Genes with Biomimetically Mineralized Zeolitic Imidazolate Framework-8 (ZIF-8). *Small* **2019**, *15* (36), No. e1902268.
(40) Acharya, G.; Shin, C. S.; Vedantham, K.; McDermott, M.; Rish, T.; Hansen, K.; Fu, Y.; Park, K. A study of drug release from homogeneous PLGA microstructures. *J. Controlled Release* **2010**, *146* (2), 201−6.
(41) Azevedo, M. C. S.; Fonseca, A. C.; Colavite, P. M.; Melchiades, J. L.; Tabanez, A. P.; Codo, A. C.; de Medeiros, A. I.; Trombone, A. P. F.; Garlet, G. P. Macrophage Polarization and Alveolar Bone Healing Outcome: Despite a Significant M2 Polarizing Effect, VIP and PACAP Treatments Present a Minor Impact in Alveolar Bone Healing in Homeostatic Conditions. *Front Immunol* **2021**, *12*, No. 782566.
(42) Agibalova, T.; Hempel, A.; Maurer, H. C.; Ragab, M.; Ermolova, A.; Wieland, J.; Waldherr Ávila de Melo, C.; Heindl, F.; Giller, M.; Fischer, J. C.; Tschurtschenthaler, M.; Kohnke-Ertel, B.; Öllinger, R.; Steiger, K.; Demir, I. E.; Saur, D.; Quante, M.; Schmid, R. M.; Middelhoff, M. Vasoactive intestinal peptide promotes secretory differentiation and mitigates radiation-induced intestinal injury. *Stem Cell Res. Ther.* **2024**, *15* (1), 348.
(43) Cetik, R. M.; Yabanoglu Ciftci, S.; Arica, B.; Baysal, I.; Akarca Dizakar, S. O.; Erbay Elibol, F. K.; Gencer, A.; Demir, T.; Ayvaz, M. Evaluation of the Effects of Transforming Growth Factor-Beta 3 (TGF-beta3) Loaded Nanoparticles on Healing in a Rat Achilles Tendon Injury Model. *Am. J. Sports Med.* **2022**, *50* (4), 1066−1077.
(44) Liu, Y.; Wang, L.; Li, S.; Zhang, T.; Chen, C.; Hu, J.; Sun, D.; Lu, H. Mechanical stimulation improves rotator cuff tendon-bone healing via activating IL-4/JAK/STAT signaling pathway mediated macrophage M2 polarization. *J. Orthop Translat* **2022**, *37*, 78−88.
(45) Lui, P. P.; Wong, O. T.; Lee, Y. W. Transplantation of tendon-derived stem cells pre-treated with connective tissue growth factor and ascorbic acid in vitro promoted better tendon repair in a patellar tendon window injury rat model. *Cytotherapy* **2016**, *18* (1), 99−112.
(46) Mandla, S.; Davenport Huyer, L.; Wang, Y.; Radisic, M. Macrophage Polarization with Angiopoietin-1 Peptide QHREDGS. *ACS Biomater Sci. Eng.* **2019**, *5* (9), 4542−4550.
(47) Yang, J.; Zhang, X.; Lu, B.; Mei, J.; Xu, L.; Zhang, X.; Su, Z.; Xu, W.; Fang, S.; Zhu, C.; Xu, D.; Zhu, W. Inflammation-Responsive Hydrogel Spray for Synergistic Prevention of Traumatic Heterotopic

https://doi.org/10.1021/acsnano.4c16917
ACS Nano 2025, 19, 13871−13888

Ossification via Dual-Homeostatic Modulation Strategy. *Adv. Sci.* **2023**, *10* (30), No. e2302905.
(48) Chen, Y.; Wang, T.; Liang, F.; Han, J.; Lou, Z.; Yu, Y.; Li, J.; Zhan, T.; Gu, Y.; Dong, L.; Jiang, B.; Zhang, W.; Wu, M.; Lu, Y. Nicotinamide phosphoribosyltransferase prompts bleomycin-induced pulmonary fibrosis by driving macrophage M2 polarization in mice. *Theranostics* **2024**, *14* (7), 2794−2815.
(49) Yao, Q.; Zheng, X.; Zhang, X.; Wang, Y.; Zhou, Q.; Lv, J.; Zheng, L.; Lan, J.; Chen, W.; Chen, J.; Chen, D. METTL3 Potentiates M2Macrophage-Driven MMT to Aggravate Renal Allograft Fibrosis via the TGF-beta1/Smad3 Pathway. *Adv. Sci.* **2025**, No. e2412123.
(50) Wynn, T. A.; Vannella, K. M. Macrophages in Tissue Repair, Regeneration, and Fibrosis. *Immunity* **2016**, *44* (3), 450−462.
(51) Xu, H.; Zhu, Y.; Hsiao, A. W.; Xu, J.; Tong, W.; Chang, L.; Zhang, X.; Chen, Y. F.; Li, J.; Chen, W.; Zhang, Y.; Chan, H. F.; Lee, C. W. Bioactive glass-elicited stem cell-derived extracellular vesicles regulate M2 macrophage polarization and angiogenesis to improve tendon regeneration and functional recovery. *Biomaterials* **2023**, *294*, No. 121998.
(52) Schoenenberger, A. D.; Tempfer, H.; Lehner, C.; Egloff, J.; Mauracher, M.; Bird, A.; Widmer, J.; Maniura-Weber, K.; Fucentese, S. F.; Traweger, A.; Silvan, U.; Snedeker, J. G. Macromechanics and polycaprolactone fiber organization drive macrophage polarization and regulate inflammatory activation of tendon in vitro and in vivo. *Biomaterials* **2020**, *249*, No. 120034.
(53) Tajbakhsh, A.; Rezaee, M.; Kovanen, P. T.; Sahebkar, A. Efferocytosis in atherosclerotic lesions: Malfunctioning regulatory pathways and control mechanisms. *Pharmacol Ther* **2018**, *188*, 12−25.
(54) Chen, J.; Sheng, R.; Mo, Q.; Backman, L. J.; Lu, Z.; Long, Q.; Chen, Z.; Cao, Z.; Zhang, Y.; Liu, C.; Zheng, H.; Qi, Y.; Cao, M.; Rui, Y.; Zhang, W. Controlled TPCA-1 delivery engineers a pro-tenogenic niche to initiate tendon regeneration by targeting IKKbeta/NF-kappaB signaling. *Bioact Mater.* **2025**, *44*, 319−338.
(55) Wang, Q.; Jiang, H.; Li, Y.; Chen, W.; Li, H.; Peng, K.; Zhang, Z.; Sun, X. Targeting NF-kB signaling with polymeric hybrid micelles that co-deliver siRNA and dexamethasone for arthritis therapy. *Biomaterials* **2017**, *122*, 10−22.
(56) Nagashima, H.; Mahlakõiv, T.; Shih, H. Y.; Davis, F. P.; Meylan, F.; Huang, Y.; Harrison, O. J.; Yao, C.; Mikami, Y.; Urban, J. F.; Caron, K. M.; Belkaid, Y.; Kanno, Y.; Artis, D.; O'Shea, J. J. Neuropeptide CGRP Limits Group 2 Innate Lymphoid Cell Responses and Constrains Type 2 Inflammation. *Immunity* **2019**, *51* (4), 682−695.
(57) Hoeffel, G.; Debroas, G.; Roger, A.; Rossignol, R.; Gouilly, J.; Laprie, C.; Chasson, L.; Barbon, P. V.; Balsamo, A.; Reynders, A.; Moqrich, A.; Ugolini, S. Sensory neuron-derived TAFA4 promotes macrophage tissue repair functions. *Nature* **2021**, *594* (7861), 94−99.
(58) Ackermann, P. W.; Ahmed, M.; Kreicbergs, A. Early nerve regeneration after achilles tendon rupture–a prerequisite for healing? A study in the rat. *J. Orthop Res.* **2002**, *20* (4), 849−56.
(59) Lee, W. L.; Slutsky, A. S. A negative trial for vasoactive intestinal peptide in COVID-19-associated acute hypoxaemic respiratory failure. *Lancet Respir Med.* **2023**, *11* (9), 759−760.
(60) Ackermann, P. W.; Franklin, S. L.; Dean, B. J.; Carr, A. J.; Salo, P. T.; Hart, D. A. Neuronal pathways in tendon healing and tendinopathy–update. *Front Biosci (Landmark Ed)* **2014**, *19* (8), 1251−78.
(61) Brown, S. M.; Barkauskas, C. E.; Grund, B.; Sharma, S.; Phillips, A. N.; Leither, L.; Peltan, I. D.; Lanspa, M.; Gilstrap, D. L.; Mourad, A.; Lane, K.; Beitler, J. R.; Serra, A. L.; Garcia, I.; Almasri, E.; Fayed, M.; Hubel, K.; Harris, E. S.; Middleton, E. A.; Barrios, M. A. G.; Mathews, K. S.; Goel, N. N.; Acquah, S.; Mosier, J.; Hypes, C.; Salvagio Campbell, E.; Khan, A.; Hough, C. L.; Wilson, J. G.; Levitt, J. E.; Duggal, A.; Dugar, S.; Goodwin, A. J.; Terry, C.; Chen, P.; Torbati, S.; Iyer, N.; Sandkovsky, U. S.; Johnson, N. J.; Robinson, B. R. H.; Matthay, M. A.; Aggarwal, N. R.; Douglas, I. S.; Casey, J. D.; Hache-Marliere, M.; Georges Youssef, J.; Nkemdirim, W.; Leshnower, B.; Awan, O.; Pannu, S.; O'Mahony, D. S.; Manian, P.; Awori Hayanga, J. W.; Wortmann, G. W.; Tomazini, B. M.; Miller, R. F.; Jensen, J. U.; Murray, D. D.; Bickell, N. A.; Zatakia, J.; Burris, S.; Higgs, E. S.; Natarajan, V.; Dewar, R. L.; Schechner, A.; Kang, N.; Arenas-Pinto, A.; Hudson, F.; Ginde, A. A.; Self, W. H.; Rogers, A. J.; Oldmixon, C. F.; Morin, H.; Sanchez, A.; Weintrob, A. C.; Cavalcanti, A. B.; Davis-Karim, A.; Engen, N.; Denning, E.; Taylor Thompson, B.; Gelijns, A. C.; Kan, V.; Davey, V. J.; Lundgren, J. D.; Babiker, A. G.; Neaton, J. D.; Lane, H. C.; ACTIV-3b/Therapeutics for Severely Ill Inpatients with COVID-19 (TESICO) Study Group. Intravenous aviptadil and remdesivir for treatment of COVID-19-associated hypoxaemic respiratory failure in the USA (TESICO): a randomised, placebo-controlled trial. *Lancet Respir. Med.* **2023**, *11* (9), 791−803.
(62) Sun, X.; Guo, C.; Zhao, F.; Zhu, J.; Xu, Y.; Liu, Z. Q.; Yang, G.; Zhang, Y. Y.; Gu, X.; Xiao, L.; Liu, Z.; Yang, P. C. Vasoactive intestinal peptide stabilizes intestinal immune homeostasis through maintaining interleukin-10 expression in regulatory B cells. *Theranostics* **2019**, *9* (10), 2800−2811.
(63) Zhou, Y.; Zhang, C. Y.; Duan, J. X.; Li, Q.; Yang, H. H.; Sun, C. C.; Zhang, J.; Luo, X. Q.; Liu, S. K. Vasoactive intestinal peptide suppresses the NLRP3 inflammasome activation in lipopolysaccharide-induced acute lung injury mice and macrophages. *Biomed Pharmacother* **2020**, *121*, No. 109596.
(64) Korkmaz, O. T.; Ay, H.; Aytan, N.; Carreras, I.; Kowall, N. W.; Dedeoglu, A.; Tuncel, N. Vasoactive Intestinal Peptide Decreases beta-Amyloid Accumulation and Prevents Brain Atrophy in the 5xFAD Mouse Model of Alzheimer's Disease. *J. Mol. Neurosci* **2019**, *68* (3), 389−396.
(65) de Souza, F. R. O.; Ribeiro, F. M.; Lima, P. M. D. Implications of VIP and PACAP in Parkinson's Disease: What do we Know So Far? *Curr. Med. Chem.* **2021**, *28* (9), 1703−1715.
(66) Li, Y.; Li, H.; Wang, L.; Xie, W.; Yuan, D.; Wen, Z.; Zhang, T.; Lai, J.; Xiong, Z.; Shan, Y.; Jiang, W. The p65-LOC727924-miR-26a/KPNA3-p65 regulatory loop mediates vasoactive intestinal peptide effects on osteoarthritis chondrocytes. *Int. Immunopharmacol* **2023**, *122*, No. 110518.

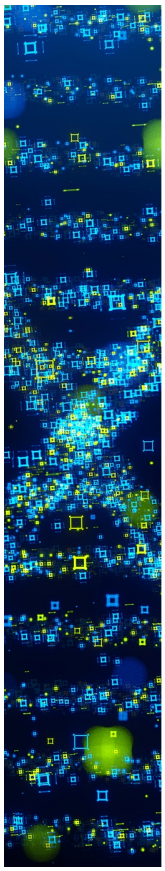
CAS BIOFINDER DISCOVERY PLATFORM™
STOP DIGGING THROUGH DATA —START MAKING DISCOVERIES
CAS BioFinder helps you find the right biological insights in seconds
Start your search
CAS
A division of the American Chemical Society

https://doi.org/10.1021/acsnano.4c16917
ACS Nano 2025, 19, 13871−13888